NIST Technical Note 1470

NIST Measurement Services: Fast Repetitive Pulse Transition Parameters, 50 Ω

Donald R. Larson
Nicholas G. Paulter, Jr.

NIST National Institute of Standards and Technology • Technology Administration • U.S. Department of Commerce

NIST Technical Note 1470

NIST Measurement Services: Fast Repetitive Pulse Transition Parameters, 50 Ω

Donald R. Larson
Nicholas G. Paulter, Jr.
Electronics and Electrical Engineering laboratory
Quantum Electrical Metrology Division

May 2005

U.S. Department of Commerce
Carlos M. Gutierrez, Secretary

Technology Administration
Phillip J. Bond, Under Secretary for Technology

National Institute of Standards and Technology
Hratch G. Semerjian, Acting Director

National Institute of Standards and Technology Technical Note 1470
Natl. Inst. Stand. Technol. Tech.. Note 1470, 56 pages (May 2005)
CODEN: NTNOEF

U.S. GOVERNMENT PRINTING OFFICE
WASHINGTON: 2005

For sale by the Superintendent of Documents, U.S. Government Printing Office
Internet: bookstore.gpo.gov — Phone: (202) 512-1800 — Fax: (202) 512-2250
Mail: Stop SSOP, Washington, DC 20402-0001

Table of Contents

List of Tables

List of Figures

NIST Measurement Services: Fast Repetitive Pulse Transition Parameters, 50 Ω

Donald R. Larson and Nicholas G. Paulter, Jr.

ABSTRACT This document describes the Special Test 65200S, "Fast Repetitive Pulse Transition Parameters, 50 Ω." This special test service is used to acquire the parameters: pulse transition and amplitude of fast repetitive pulses.

1. Description of Measurement Service

The 65200S is optimized for measuring certain parameters of waveforms corresponding to very fast transition pulses, where the transition durations of these pulses are less than 350 ps (or equivalently, the 3 dB attenuation bandwidth of the pulse is greater than 1 GHz). These pulses can also represent the step response of high-speed samplers. An example of a measured waveform is shown in Figure 1-1.

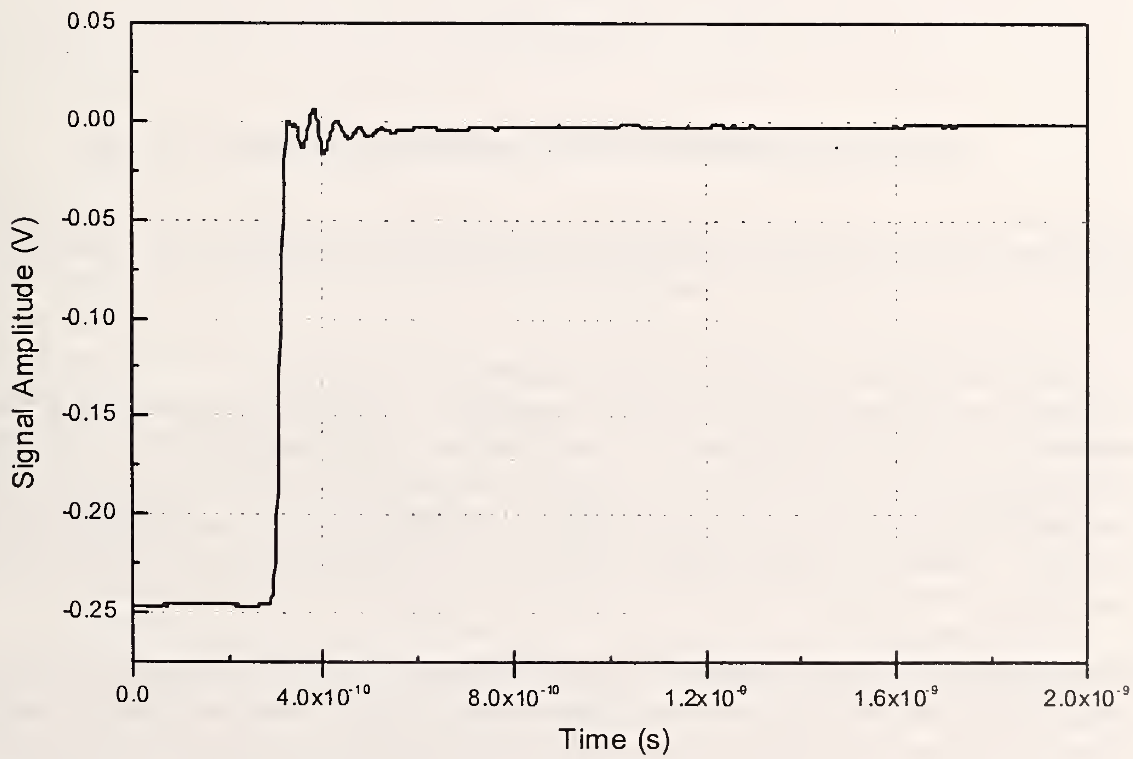

Figure 1-1. Typical waveform measured under 65200S.

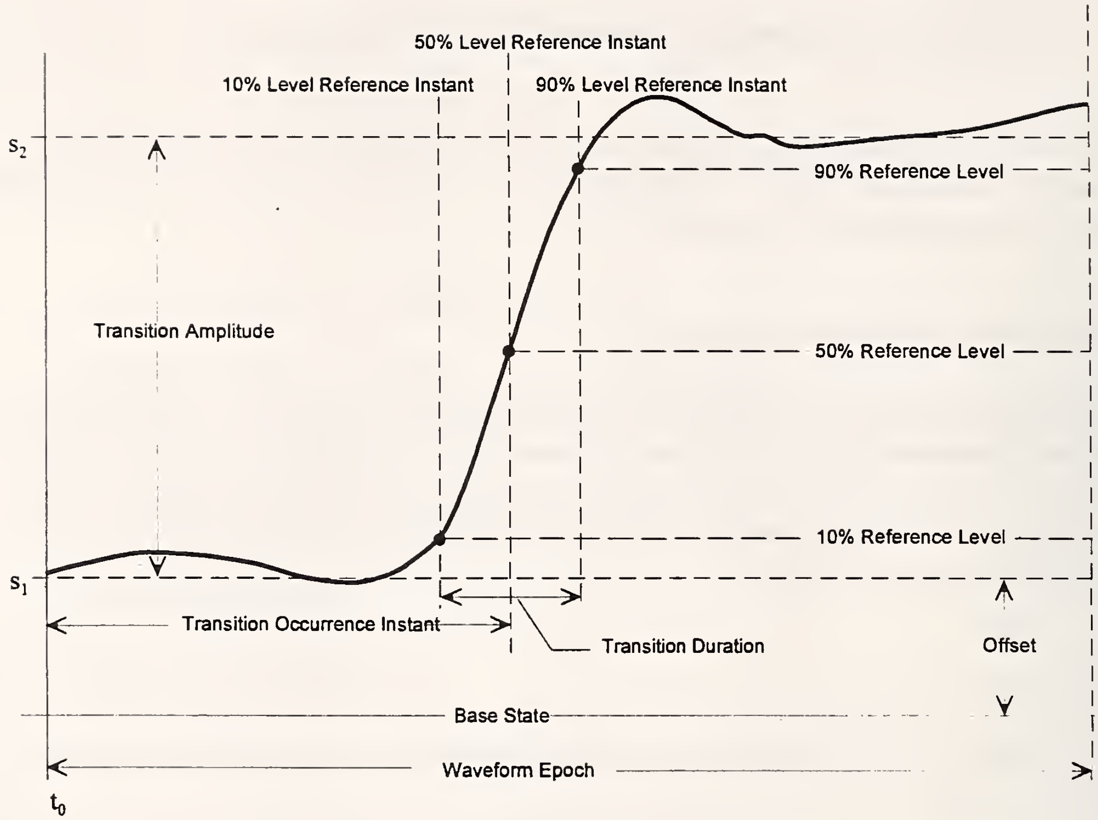

Figure 1-2. Definition of pulse amplitude and transition duration.

A brief description of this measurement service is provided in [1]. The service is currently performed using the Waveform Parameter Analysis System (WPAS).

1.1 Quantities Measured, Ranges, and Expanded Uncertainties

The parameters provided by this service are: waveform or transition amplitude, transition duration, overshoot and undershoot. The amplitude is typically reported in volts, the transition duration (both 10 % to 90 % and 20 % to 80 %) is reported in seconds, and the undershoot and overshoot are in percent of waveform amplitude. The parameters are best described by Figures 1-2 and 1-3. These parameters conform to the definitions and descriptions contained in IEEE Standard 181-2003 [2].

The definition of amplitude as given in the IEEE Standard 181-2003 is "the level of the state succeeding a transition minus the level of the state preceding the same transition." Transition duration is defined as the difference between two instants on the waveform, these instants occurring when the waveform crosses certain user-defined reference levels, such as the 10 % and 90 % reference levels.

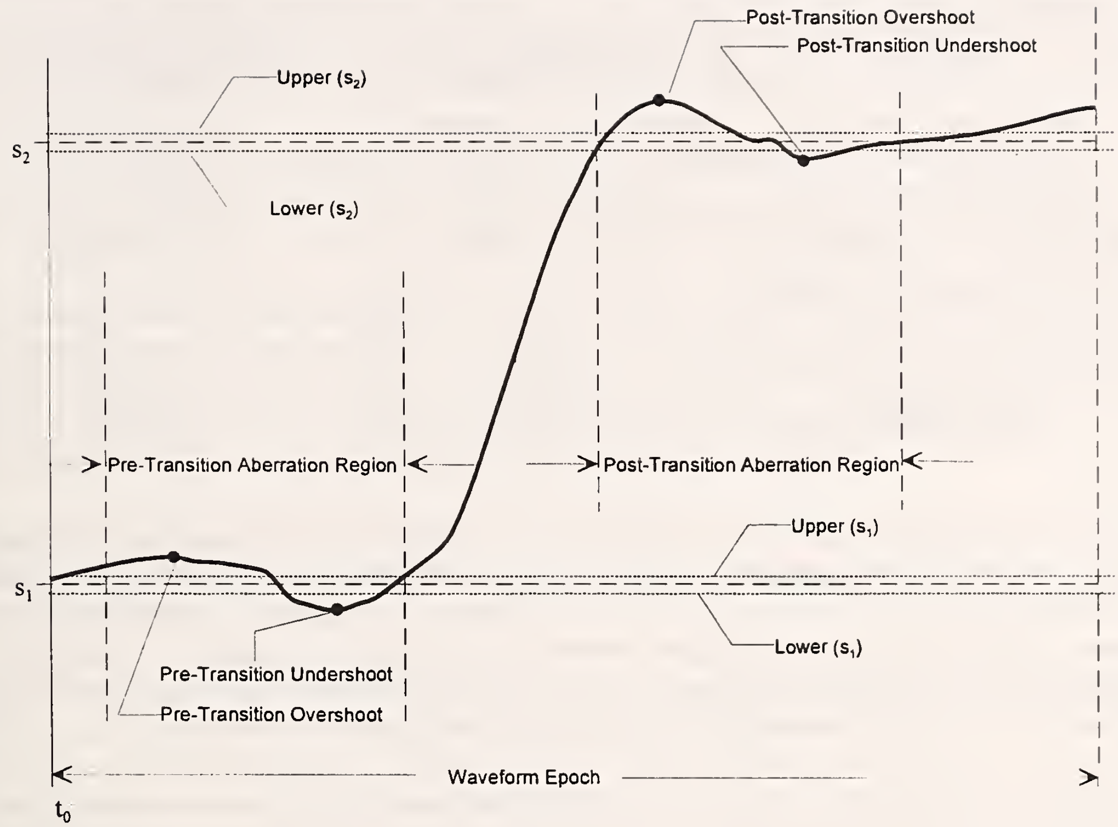

Figure 1-3. Definition of overshoot and undershoot.

The parameters of undershoot and overshoot have historically been subject to interpretation and, without further clarification, are considered deprecated terms in Reference 2. The most common usage of undershoot and overshoot refer to what is now defined as the pre-transition undershoot and post-transition overshoot [2]. There is also pre-transition overshoot and post-transition undershoot; this gives a total of four "shoot"-related terms. In Figure 1-3, the Post-Transition Aberration Region is defined in [2] to be that period between the 50 % reference level instant ($t_{50\%}$) and $t_{50\%} + 3t_d$ where t_d is the transition duration. The Pre-Transition Aberration Region is similarly defined ($t_{50\%} - 3t_d$). Overshoot and undershoot (the deprecated terms) were once included in this service but were dropped for lack of a suitable uncertainty analysis. The four "shoot"-related terms were recently introduced into the 65200S after completion of a new uncertainty analysis, automation of the uncertainty analysis calculation, and analysis of a sufficient number of 65200S tests. The algorithms used to obtain these parameters also conform to the IEEE standard. The parameters, ranges, and expanded uncertainties for the 65200S are listed in Table 1-1. Notes are shown after the table.

Table 1-1. Uncertainty for Calibration of Fast Repetitive Pulse Transition Parameters

Parameter	Parameter Range	Typical Expanded Uncertainty
Pulse Amplitude (A)	-400 mV ≤ A ≤ 400 mV	1.0 mV + 1.4ΔA [1]
Transition Duration (t_d)	5 ps ≤ t_d ≤ 100 ns	1.25 ps + 0.1 Δt [2]
Pulse Duration (t_P) (between 50 % reference level instants)	10 ps ≤ t_P ≤ 100 ns	1.8 ps + 0.14Δt
Pulse Overshoot	≤ 50 %	2 % [3]
Pulse Undershoot	≤ 50 %	2 % [3]

Notes:
[1]ΔA is the amplitude discretization interval and is calculated using the full-scale amplitude range set on the sampler (for example, the full scale amplitude range is 100 mV for an amplitude sensitivity setting of 10 mV/div and a full scale display of 10 vertical divisions) and effective number of bits of the analog-to-digital converter at the input of the sampler. The effective number of bits is based on the actual number of bits of the converter and signal averaging where the noise level exceeds the range of the least significant bit of the converter.

[2]Δt is the sampling interval, that is, the interval between sampling instances, used during acquisition of the DUT waveform. For example, a waveform epoch of 1 ns where the waveform contains 1000 elements gives a sampling interval of 1 ps.

[3]By definition, undershoot and overshoot are positive values, therefore, the lower uncertainty bound is limited to a value such that undershoot and overshoot are greater than 0 %.

1.2 Types of Artifact or Transfer Standards
To be acceptable for calibration, the customer's pulse generator must meet the criteria outlined in the following list.

1. The device must provide a trigger output with a repetition rate between 10 Hz and 2 GHz. Alternatively, NIST can provide a range of trigger signals, however, in this case, the customer's pulse generator must be able to be driven at a rate between 10 Hz and 2 GHz.

2. The customer's device must have a nominal output impedance of 50 Ω.

3. The customer's device must have a precision coaxial output connector, such as, an SMA, GPC-7, Type N, GPC-3.5, etc. Note, the NIST WPAS input uses a 2.4 mm (female) coaxial connector. Consequently, the measured response of the submitted device using any other coaxial connector will contain the effects of any necessary adapters.

4. The maximum input signal amplitude (including overshoot and undershoot) that is measurable without attenuators is 800 mV. For pulses with greater pulse amplitudes, the customer shall supply an attenuator to decrease the pulse amplitude to 800 mV or less. The permissible dc offset (without attenuators) is ± 500 mV.

5. The minimum pulse transition duration must be greater than or equal to 5 ps.

6. The pulse duration is only measured for rectangular pulses or impulse-like pulses.

If the customer's device is a sampling head, it must either be compatible with existing NIST-owned oscilloscope mainframes (Tektronix 11801, TDS 8000, HP 54120, HP 54750, and Agilent 86100A)[1] or the customer must provide a compatible mainframe. If the customer provides the mainframe, the customer must make provision for transfer of the data acquired by the oscilloscope to the PC compatible computer of the WPAS for analysis.

1.3 Shipping and Handling Instructions

All aspects of shipping (both receipt from and returning to the customer) are arranged through the responsible NIST personnel.

Pulse generators and samplers are static sensitive and should only be handled on electro-static discharge (ESD) protective surfaces and while wearing a wrist strap or other means of controlling static discharge. The WPAS sits on an ESD work surface and ESD wrist straps are located at multiple points around and on this work surface.

---

[1]Certain commercial equipment, instruments, or materials are identified in this paper to foster understanding. Such identification does not imply recommendation or endorsement by the National Institute of Standards and Technology, nor does it imply that the materials or equipment identified are necessarily the best available for the purpose.

2. Design Philosophy

The purpose of the 65200S is to provide pulse parameters (pulse amplitude, transition duration, overshoot, and undershoot), as defined by national and international standards [2,3], of waveforms containing one or two fast transitions and two states (such as the high and low states). The methods used in the 65200S for computing the values of these parameters are also defined by national and international standards [2,3]. The waveforms obtained with the 65200S can be either those taken from the output of a customer's pulse generator and measured with a WPAS sampler or those taken from the output of a WPAS pulse generator and measured with a customer's sampler. To measure the step response of high-speed samplers, the 65200S uses pulse generators with known outputs. To measure the output of high-speed pulse generators, the 65200S uses samplers with known impulse responses.

Instruments used to measure dc and steady-state values, such as voltmeters, signal analyzers, and spectrum analyzers, cannot be used in the 65200S because the 65200S is used to measure transition-related parameters of pulse waveforms. Instruments for measuring high speed transitions must be used to accomplish the requirements for the 65200S, and the only instruments that satisfy these requirements are high-speed waveform recorders (real time and sampling oscilloscopes). In particular, the 65200S uses high-speed equivalent-time samplers, with a step response transition duration < 5 ps (or, equivalently, a 3 dB attenuation bandwidth > 70 GHz). Current state-of-the-art real time oscilloscopes do not have the bandwidth (impulse response) necessary to measure high-speed pulse parameters.

2.1 Physical Principles of Sampler Structures

The voltage pulse that is input to the WPAS sampler is sampled as it propagates down a transmission line. The sampling elements are in contact with the transmission line but have a much higher electrical impedance (> 1 kΩ) than that of the transmission line (nominally 50 Ω). Consequently, the effect of the sampling element is negligibly small (100 times less than the published uncertainty values) and, if desired, can be computed based on a simple voltage divider network. The sampler and the transmission line are incorporated into one unit and are not typically separable. The voltage or current of the pulse is sampled as it propagates down the transmission line, and this sampled voltage or current is used to construct the pulse's waveform.

The sampled waveform of the pulse is presently obtained using an equivalent-time sampling process. In this process, the sampling element is activated by a trigger pulse at specific instants relative to the pulse being measured. Typically only one instant on the waveform is obtained for each trigger pulse, and the waveform datum corresponding to this instant may be the result of more than one sampled event. The waveform is constructed by concatenating the waveform data from successive sampling instants. This sampling process requires a repetitive stationary pulse signal. Deviation of the pulse from stationarity results in an increase in trigger jitter and amplitude noise. The effect of jitter is compensated and the effect of both the jitter and noise are considered components in the uncertainty analysis (see Section 5).

Sampling structures include, but are not limited to, semiconductor diodes, superconducting

Josephson junction devices, electrooptic and photoconductive devices. Semiconductor diodes are the mainstay of sampling instruments because they can be implemented using all solid state technology, whereas electrooptic and photoconductive methods require, in addition to solid state technology, ultrashort pulsed laser technology. Semiconductor diodes provide a sampled voltage waveform of the pulse. This voltage waveform is obtained by strobing the diode with an electrical pulse. The instant the strobe is being applied to the diode, the forward resistance of the diode decreases and a replica of the pulse at that instant passes through the diode to a hold circuit. The magnitude and duration of the replica is dependent on the magnitude and duration of the strobe pulse, the switching behavior of the diode, and the material properties of the diode (see [4,5] for example, for information on diode operation).

Josephson junctions are metal-insulator-metal devices that are cooled until the metal becomes superconducting. If the insulator, usually an oxide, is sufficiently thin, current may tunnel through the insulating barrier. This device may switch between zero and finite voltage states in a few picoseconds [6]. Hypres, Inc. manufactured and marketed a digital sampling oscilloscope using a Josephson junction based sampler from 1987 until 1990. The impulse response duration was approximately 5 ps, the 3dB attenuation bandwidth was 70 GHz and the sampler was cooled using liquid helium.

Electro-optic devices provide a sampled voltage waveform of the pulse. This voltage waveform is obtained through the interaction of the electric field of the propagating pulse with laser light in an electrooptic material. The applied electric field modulates the refractive index of the electrooptic material usually through the Pockels Effect. This index modulation can be measured with an appropriate optical system by observing a change in optical intensity [7]. This process has resulted in several different sampling instruments[8-10], one of which is used routinely for high-speed pulse measurements [11].

Photoconductive devices provide a sampled current waveform of the pulse. The current waveform is obtained by extracting charge from the propagating pulse. The charge is extracted when the sampling gate is excited (turned on) (for examples, see [12-15]). The amount of charge extracted and the effect of the sampling process on the propagating pulse are dependent on the on-state resistance of the photoconductor [16]. Several measurement systems have been developed using this technology [12,17,18].

2.2 History

NIST has offered the transition duration special test service since before July 24, 1970 when the first special test was performed. Dr. Norris S. Nahman, Section Chief of the Pulse and Time Domain Section in the Electromagnetics Division (272.20), oversaw the introduction of the pulse parameter measurements at NIST (then NBS). R. M. Jickling performed this first test on a Tektronix model 067-0513-00 tunnel diode pulse generator. Rockwell was the customer and they were charged $130 for the service. The reported transition duration of that first test was 21 ps ±3 ps. Today, the fee for this service, provided "at cost," is typically $2400. For the majority of the tests performed, the transition durations are approximately 15 ps ± 1.25 ps. Table

2-1 lists the personnel and the managing NBS/NIST divisions.

Table 2-1. Personnel and Organizational History.

Calibration Leader (CL) or Authorized User (AU)	Date	NBS/NIST Division
R.M. Jickling (CL)	1970 - 1972	272
W. L. Gans (CL)	1973 - 1995	272, 276, 724, 723, 813, 811
J. R. Andrews (AU)	1976 - 1980	276, 724
L. A. Terrell (AU)	1988	723
S. M. Chesnut (AU)	1989	723
C. A. Jones (AU)	1990	723
N. G. Paulter (AU)	1990 - present	723, 813, 811, 817
J. P. Deyst (CL)	1995 - 1998	811
D. R. Larson (CL)	1998 - present	811, 817

At the inception of the 65200S service in 1970, the decision was made to use commercially available oscilloscopes to perform the measurements. Although commercially available oscilloscopes are still used in the performance of the 65200S, because they are easy to operate and the measured waveforms may be easily transferred to computers for data analysis, this is not a requirement for the 65200S. If used, the commercial oscilloscope must be fully characterized to determine the uncertainty in the measurement results. The most important characteristic of the sampling head is its impulse response. Almost all commercial sampling oscilloscopes have used semiconductor diodes in their samplers. The measured waveform is the convolution of the input signal and the impulse response of the sampling head. Since every sampling head has a finite duration sampling aperture and thus, a finite bandwidth, the measured transition duration will be slower than the transition duration of the input signal. If the impulse response of the sampling head can be determined, it can be deconvolved from the measured signal to yield a more accurate estimate of the input signal. Over the years, the 65200S has used either the modeling or characterization of the sampler to determine its impulse response. In addition to the impulse response, the vertical gain, the horizontal axis or timebase error, and the temperature dependence of the impulse response and vertical gain need to be characterized. The pulse generator, which provides a known output pulse, requires calibration of its output pulse amplitude, transition duration, and aberrations.

In 1970, a Hewlett-Packard (HP, now Agilent) 181A oscilloscope with an HP 1815 sampling head and later an HP 1817 sampling head was used.

In 1972, NBS was using an HP 140A oscilloscope with an 1430B sampling head and the system was referred to as the APMS (Automatic Pulse Measurement System). The 3 dB attenuation bandwidth of the sampler was estimated to be 18 GHz. It was specially modified by NBS to allow waveform data transfer to a mini-computer.

From the first test in 1970 until the inauguration of the AWAMS in 1989, the impulse response of the sampling heads used in this service were obtained by modeling the sampling head circuitry. This work was done by a guest researcher at NBS, Dr. Sedki Riad [19]. The circuit model was verified by comparing predicted measurement results with actual for a variety of input signals.

In 1989, the Automatic Waveform Acquisition and Measurement System or AWAMS, incorporating an HP 54120 oscilloscope with an HP 54121A sampling head was characterized and used for performing calibrations.

The impulse response of the sampling head used in the AWAMS was determined using a different technique than the modeling techniques previously used. In the AWAMS sampler impulse estimation process, waveforms from three step generators were acquired using a commercial, superconducting sampling oscilloscope (Hypres, Inc. Picosecond Signal Processor, model PSP-1000). These Hypres-acquired waveforms were presumed to be perfect estimates of the signals produced by the step generators because the manufacturer claimed that the bandwidth of this sampler was about 70 GHz which was three and half times the bandwidth of the step generators and of the AWAMS sampling head (20 GHz). The impulse response of the AWAMS sampling head was determined by acquiring waveforms from the three step generators using the AWAMS and then deconvolving the assumed perfect step pulse estimates obtained from the superconducting sampling oscilloscope. This introduced a bias in the result and the reported uncertainty was non-symmetrical, reflecting this bias.

In 2001, to meet the above sampler requirements, NIST began using an HP 54750A oscilloscope with HP 54752A sampling heads (50 GHz bandwidth). Use of this equipment is not mandatory and any instruments with equivalent specifications can also be used. The present measurement system used in the 65200S is referred to as the Waveform Parameter Analysis System (WPAS). The impulse response estimate of the sampling heads used in the WPAS has been obtained using the "Nose-to-Nose" technique (see Section 2.4). This measurement technique is performed periodically to check the impulse response estimate of the samplers.

In 2004, NIST replaced the HP 54750A/54752A with the Agilent 86100A oscilloscope and Agilent 86118A sampling head which has a bandwidth greater than 70 GHz. This instrument has also been characterized using the "Nose-to-Nose" technique.

2.3 Impulse Response using the Nose-to-Nose Technique

This technique is only applicable when using particular diode-based sampling circuits provided by certain manufacturers. In these particular sampling circuits, if the offset level of the sampler is a value other than 0 V, the sampling head generates or "kicks out" a pulse each time it samples a signal [20,21]. It has been assumed that the pulse so generated is equivalent to the impulse response of the sampling head. We have checked that assumption and found that it introduces an uncertainty of only about 0.3 ps in the impulse response estimate of the sampling head. The Nose-to-Nose technique uses three sampling heads and two oscilloscope mainframes. The inputs of two sampling heads, each in a separate mainframe, are connected together in such a way as to make them appear "nose-to-nose." One sampling head is made to kick-out a pulse and the other sampling head is used to acquire the kick-out pulse. However, the strobe pulse, which is generated by the trigger and initiates the sampling event, feeds through the sampling diode and appears as part of the measured kick-out waveform. This can be removed since the polarity of the strobe pulse contribution does not change with the offset voltage polarity whereas the kick-out pulse contribution does. Two kick-out waveforms are acquired, one with an offset voltage polarity opposite from the other, and a difference waveform is calculated by dividing the difference of the two waveforms by two. The resulting difference waveform is an estimate of the desired kick-out pulse. Each of the three sampling heads, indicated below by the letters a, b and c, are used sequentially as a sampler and as a pulse generator. The following equations represent how the impulse response estimate is obtained from these measurements. The measurements yield three difference waveforms, ntn_{ab}, where sampler a acts as the pulse generator and sampler b as the receiver; ntn_{bc}, where sampler b acts as the pulse generator and sampler c as the receiver; and ntn_{ca}, where sampler c acts as the pulse generator and sampler a as the receiver. The "*" indicates the convolution operator:

$$\begin{aligned} ntn_{ab} &= a_g * b_r, \\ ntn_{bc} &= b_g * c_r, \\ ntn_{ca} &= c_g * a_r, \end{aligned} \tag{1}$$

where the "g" and "r" subscripts denote generator and receiver. The sampler impulse response is computed via a deconvolution process which is usually performed in the frequency domain. The spectra of the difference waveforms is given by:

$$\begin{aligned} A_g B_r &= \mathrm{F}\left\{a_g * b_r\right\}, \\ B_g C_r &= \mathrm{F}\left\{b_g * c_r\right\}, \\ C_g A_r &= \mathrm{F}\left\{c_g * a_r\right\}, \end{aligned} \tag{2}$$

where F indicates a Fourier transform. The deconvolution process involves multiplication of the spectra of two difference waveforms and division by a third difference waveform spectrum:

$$A \approx \sqrt{\frac{C_g A_r A_g B_r}{C_g B_r}},$$

$$B \approx \sqrt{\frac{A_g B_r B_g C_r}{A_g C_r}}, \tag{3}$$

$$C \approx \sqrt{\frac{B_g C_r C_g A_r}{B_g A_r}}.$$

The estimates of the impulse response of the three samplers are then found by performing the inverse Fourier transform on the A, B, and C thus found.

2.4 Timebase Characterization

In the AWAMS, which preceded the WPAS, the timebase was calibrated by applying a sinewave of known frequency to the input of the oscilloscope, measuring the time interval between zero crossings, and then comparing the length of these intervals to the expected value calculated from the known frequency. This gave the cumulative timebase error between zero crossings. The waveform was then corrected using linear interpolation. However, this process assumes the timebase errors are uniform between zero crossings.

The WPAS timebase uses a more accurate characterization method than was used for the AWAMS. The WPAS timebase is calibrated using nominally single-frequency sinusoidal signals provided by a microwave synthesized frequency source. Waveforms of these signals are acquired and errors in the timebase are derived from sinewave curve fitting techniques [22]. The synthesizer is the artifact standard and the manufacturer-claimed uncertainty in frequency uncertainty (10μHz/Hz) is used. These errors may be mapped to the time-domain via the following analysis.

$$T = N\Delta t = X\frac{1}{f_s}, \tag{4}$$

where T is the duration of the waveform epoch, N is the number of samples (data elements) in the waveform, Δt is the interval between sample instants, f_s is the input frequency provided by the source, and X is the number of cycles of f_s observed in the waveform epoch. To determine the uncertainty in T caused by uncertainty, u_{f_s} in f_s, we take the appropriate partial derivative and analyze the result. The effect of u_{f_s} on the measurement is given by:

$$u_T(f_s) = \frac{\partial T}{\partial f_s} u_{f_s} = X\frac{1}{f_s^2} u_{f_s} = T\frac{u_{f_s}}{f_s}. \tag{5}$$

The uncertainty in f_s relative to f_s is about 10μHz/Hz. Therefore, the uncertainty in the duration of the waveform epoch due to uncertainties in the reference frequency is about 10μHz/Hz. Since the waveform epoch contains between about 1000 and 4000 elements, this epoch error corresponds to about 0.04 of a sample interval. This is less than the limit imposed by amplitude noise.

2.5 Vertical Axis Calibration

The amplitude gain of the WPAS is based on comparing WPAS measurements made on a given pulse source with those made using a high-accuracy voltmeter, the NIST Sampling Waveform Analyzer (SWA [23]), on the same pulse source. The voltage accuracy of the SWA is approximately 100 times greater than that of the WPAS. Furthermore, the amplitude accuracy of the voltmeter has been compared to that of thermal voltage converters [24] on which many national metrology laboratories base ac voltage measurements. The pulse measured by the SWA is the transfer standard upon which calibration of the WPAS sampler amplitude gain is based.

The step response of the WPAS sampler is determined by measuring a reference fast-transition electrical pulse and deconvolving this known pulse from its measurement [25,26,27]. This process is also known as a waveform reconstruction process, and more will be said about the effect of this process on measurement uncertainty in Section 5. There are several ways to obtain the known electrical pulse [11,20,21]. This known electrical pulse is the artifact standard on which the step response of the WPAS sampler is calibrated. The pulse generator of the WPAS is calibrated using a sampler with a known step or impulse response. The process used in this calibration is similar to that for the sampler step response, however, in this case the sampler is the known quantity.

2.6 Physical Principles of Pulse Generators

Pulse generators can also be achieved with different technologies and methods, but the most common methods use semiconductor diodes [5]. A less commonly used method, but one that provides pulses of very short duration and with very high bandwidth is the photoconductive method [12]. Both of these methods operate similarly to those described or referenced in Section 2.1.

3. Description of System

The WPAS is depicted diagrammatically in figure 3-1. Described in this section are the performance requirements of each of the components given in Figure 3-1 and the manufacturer name and model that we are presently using to satisfy the stated requirements.

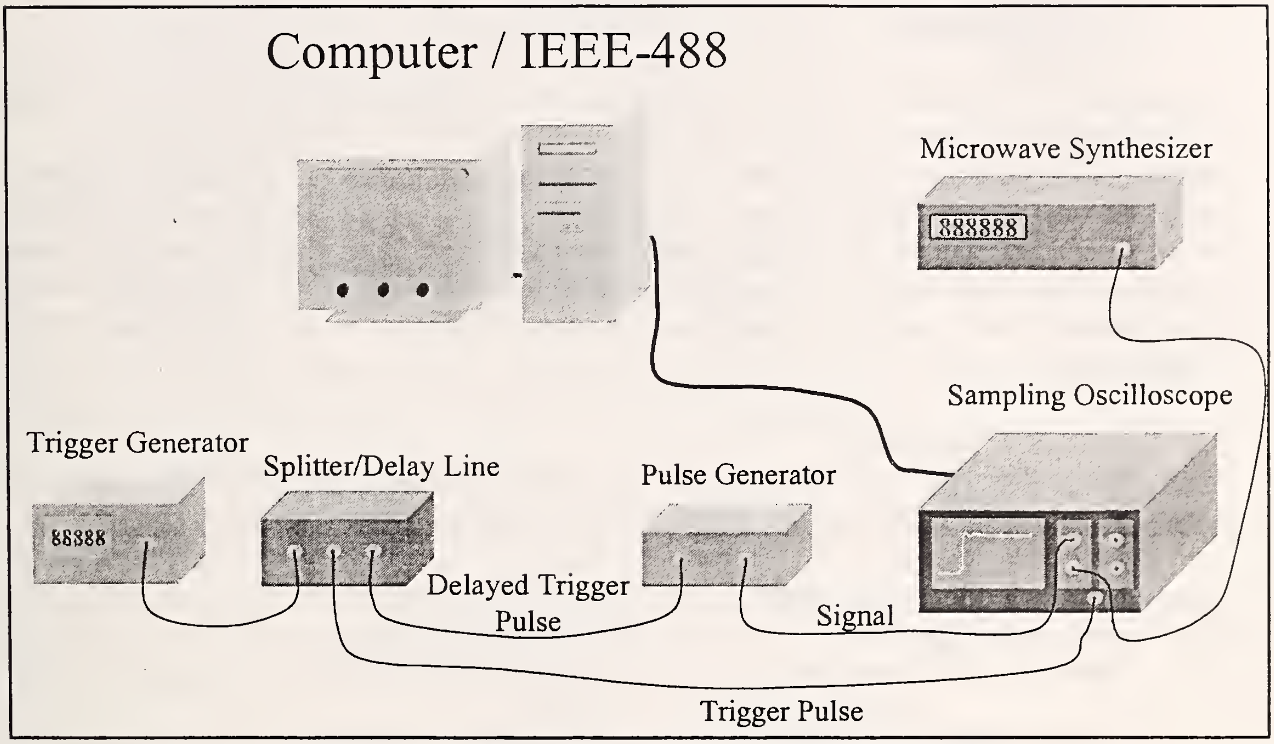

Figure 3-1. Waveform Parameter Analysis System.

This service provides characterizations of both pulse generators and sampling heads from several manufacturers. The equipment usage is slightly different depending on which is being characterized.

3.1 Trigger Generator

The trigger generator must exhibit a fast transition to minimize the introduction of jitter caused by noise on the trigger signal. It also must have sufficient amplitude to drive both the oscilloscope trigger and the pulse generator trigger after passing through the delay line/splitter.

Present performance requirements:

output pulse transition duration:	≤ 150 ps
output pulse amplitude:	≥ 2 V
output impedance:	50 Ω ± 1 Ω

The trigger generator presently used to meet these requirements is a Berkeley Nucleonics

Corporation model 6040 mainframe with a model 201E pulse generator plug-in.

3.2 Splitter/Delay Line

Present performance requirements:

delay:	22 ns to 24 ns
output impedance:	$50\ \Omega \pm 1\ \Omega$

The presently-used splitter/delay line is a packaged collection of passive coaxial devices that split the trigger pulse into two signals and delays one of the resultant trigger signals by a fixed amount. The undelayed trigger pulse is used to trigger the oscilloscope. The delayed trigger pulse is used to trigger the Pulse Generator. The delay is necessary since the oscilloscope waits a certain interval after receiving a trigger pulse before sampling. The presently-used oscilloscope requires a 22 ns trigger delay. By using this splitter/delay line instrument, the sampling head and pulse generator can be made to operate from a common trigger pulse, thereby reducing system trigger jitter.

3.3 Microwave Synthesizer

Section 2.5 outlined the application of the microwave synthesizer to the timebase characterization. Continuous wave operation is required from the microwave synthesizer.

Present performance requirements:

Frequency Range:	0.01 GHz to 26.5 GHz
Spectral Purity (Harmonics):	< -55 dBc, 0.05 to 40 GHz
(Subharmonics):	< -55 dBc
Leveled Output:	> +10 dBm

The current microwave synthesizer is a Gigatronics model 7000 that has been specially modified by the manufacturer to include a 100 MHz reference output. The microwave synthesizer is used to measure the error in the timebase of the oscilloscope. The 100 MHz reference output is used to trigger the oscilloscope and provides a lower jitter trigger signal than a 10 MHz reference output typically used on microwave synthesizers. However, the frequencies used for the timebase characterization are low enough that a 10 MHz reference would be sufficient. Other microwave synthesizers have been used and yield suitable results.

3.4 Sampler

The performance requirements for the sampler and pulse generator are near the "state-of-the-art" in commercial sampler and pulse generator technology.

Present performance requirements for the 65200S sampler are:

transition duration (10 % to 90 %):	≤ 5 ps
amplitude range:	≥ -400 mV to ≤ 400 mV
trigger jitter:	≤ 1 ps

The sampler presently used in the 65200S consists of a sampling head and oscilloscope mainframe which houses the sampling head and provides the timebase, the two most critical elements in the measurement process. The WPAS currently uses an Agilent 86100A oscilloscope mainframe and an Agilent 86118A dual channel sampling head plug-in module. The nominal 3 dB attenuation bandwidth of the sampling head is 80 GHz. The sampler selection is subject to change as the "state-of-the-art" advances. It is evident from the history provided in section 2.2 that system components have been upgraded in the past and it is anticipated that this process of upgrading will continue.

3.5 Pulse Generator

Present performance requirements for the 65200S pulse generator are:

transition duration (10 % to 90 %):	$\leq$ 5 ps
amplitude:	$\geq$ 0.2 V
trigger jitter:	$\leq$ 1 ps

Typically, the pulse generator used is a Tektronix 067-1338-00 Calibration Reference Step Generator or the kick-out pulse from an Agilent 86118A sampler.

3.6 Computer

The computer controller includes an IEEE 488 interface card that enable communications with all the equipment used in the WPAS. It is used to set up the oscilloscope and microwave synthesizer, to retrieve the waveforms acquired by the oscilloscope, and store them. It is also used to run the LabVIEW VIs (programs) that are used to calculate the deconvolution, determine the waveform parameters, and estimate the uncertainties.

3.7 Software

LabVIEW VIs have been written for many aspects of the service. Many of these have been gathered into a collection of libraries referred to as the NIST Fast Pulse Oscilloscope Calibration System (FPOCS). The FPOCS is currently used at NIST and at the U.S. Air Force Primary Standards Laboratory. The user interface for the main menu of the FPOCS software is depicted in Figure 3-2. From the main menu, the operator selects a sub-menu (see item 3 on the main menu, Figure 3-3) to perform the available operations. The menus for performing the data acquisition and temperature logging, pulse parameter calculation, timebase characterization and correction, and deconvolution are included (Figures 3-4 through 3-8). Each menu also includes an "Instructions and Help" menu containing instructions for operating this equipment and running the software (Figure 3-9).

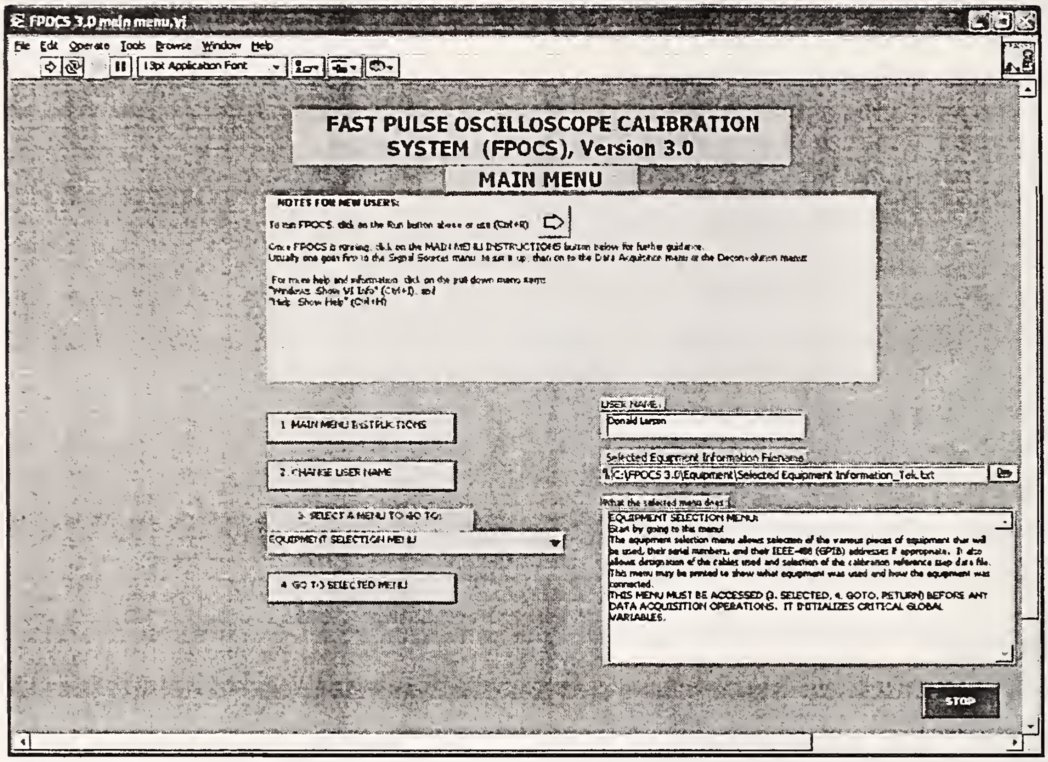

Figure 3-2. FPOCS Main Menu.

✓ EQUIPMENT SELECTION MENU
DATA ACQUISITION
WAVEFORM PLOT & STEP PARAMETERS
CONVOLUTION
STEP-STEP DECONVOLUTION
STEP-IMPULSE DECONVOLUTION
FREQUENCY RESPONSE
TIMEBASE CHARACTERIZATION
TIMEBASE ERROR CORRECTION
NOISE MEASUREMENTS
JITTER ACQUISITION
ABERRATIONS MEASUREMENT
UNCERTAINTY ANALYSIS

Figure 3-3. FPOCS Menu Selections.

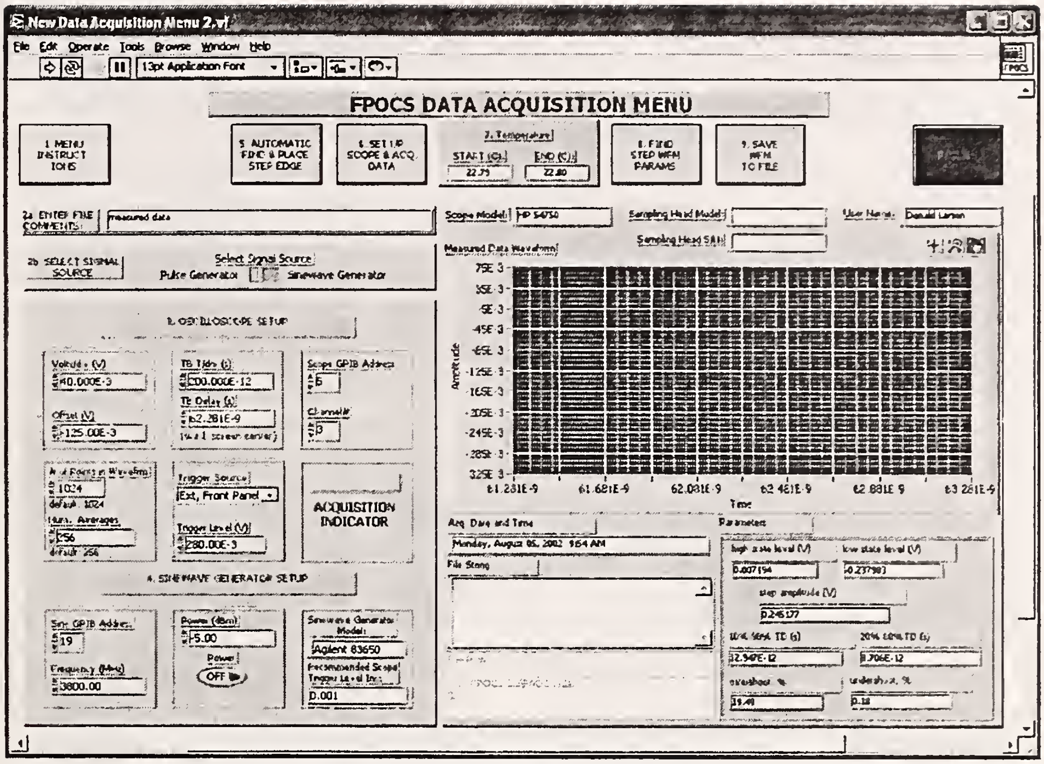

Figure 3-4. FPOCS Data Acquisition and Temperature Logging Menu.

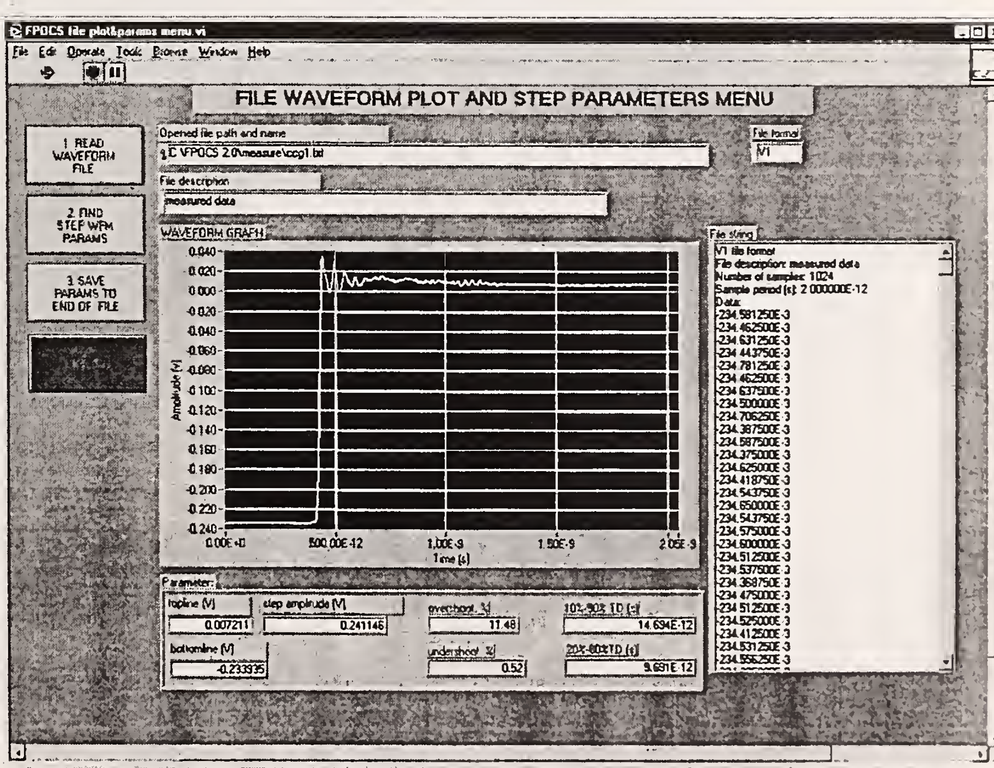

Figure 3-5. FPOCS Waveform Plot and Step Parameters Menu.

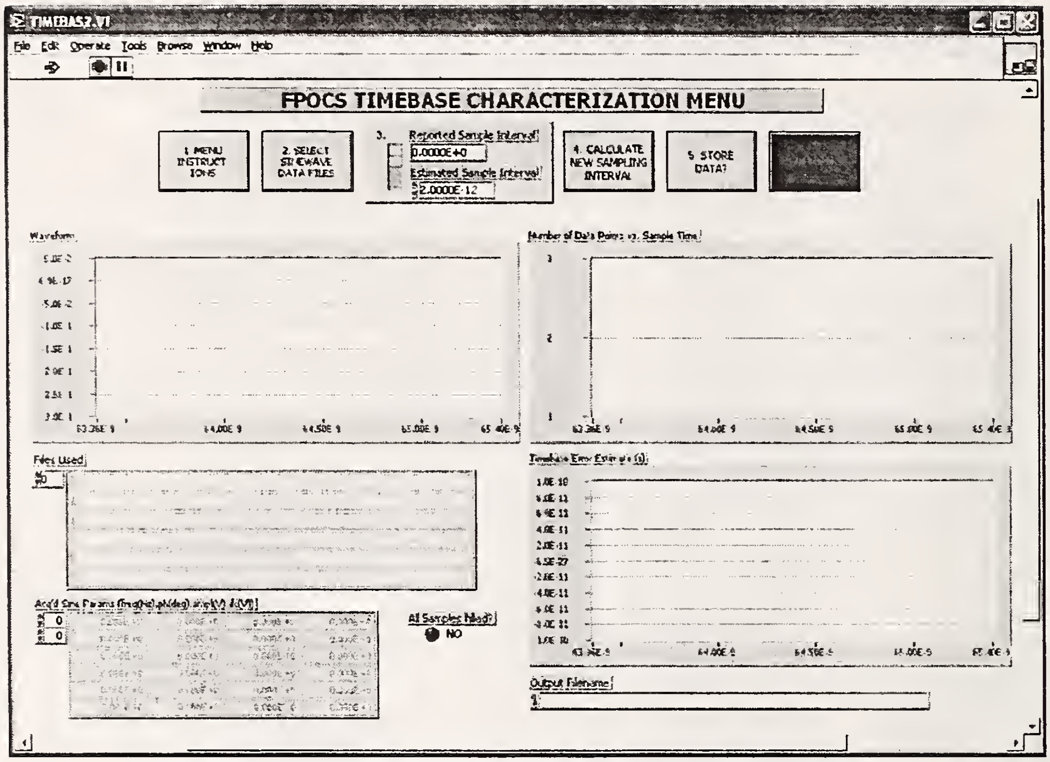

Figure 3-6. FPOCS Timebase Characterization Menu.

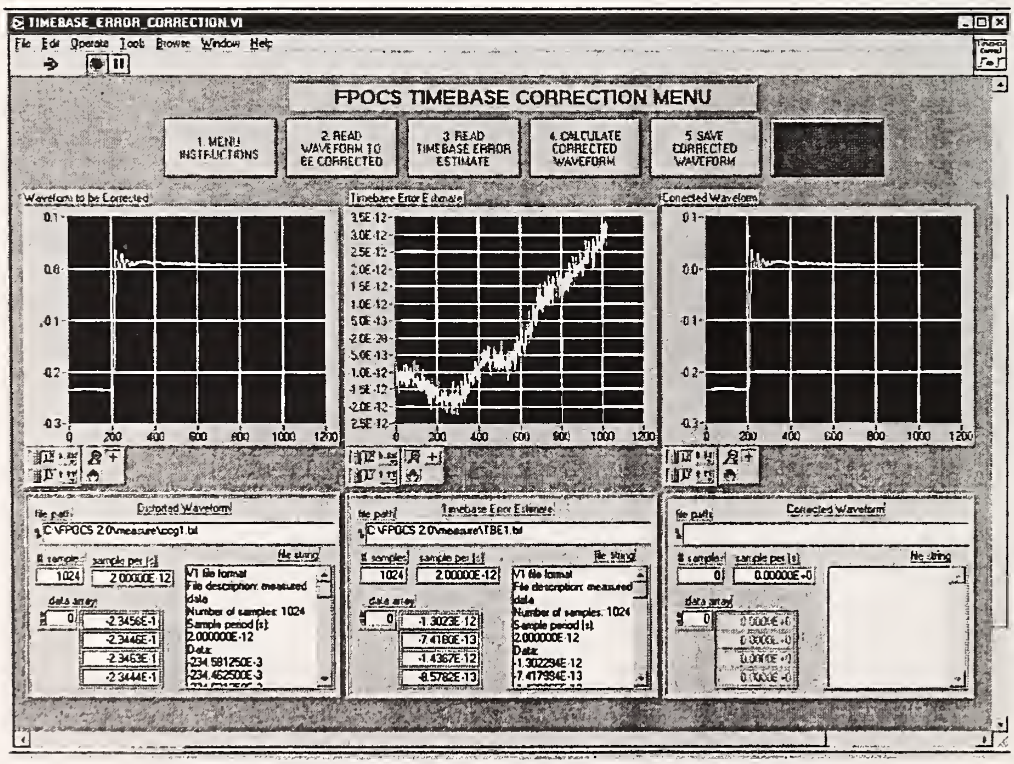

Figure 3-7. FPOCS Timebase Correction Menu.

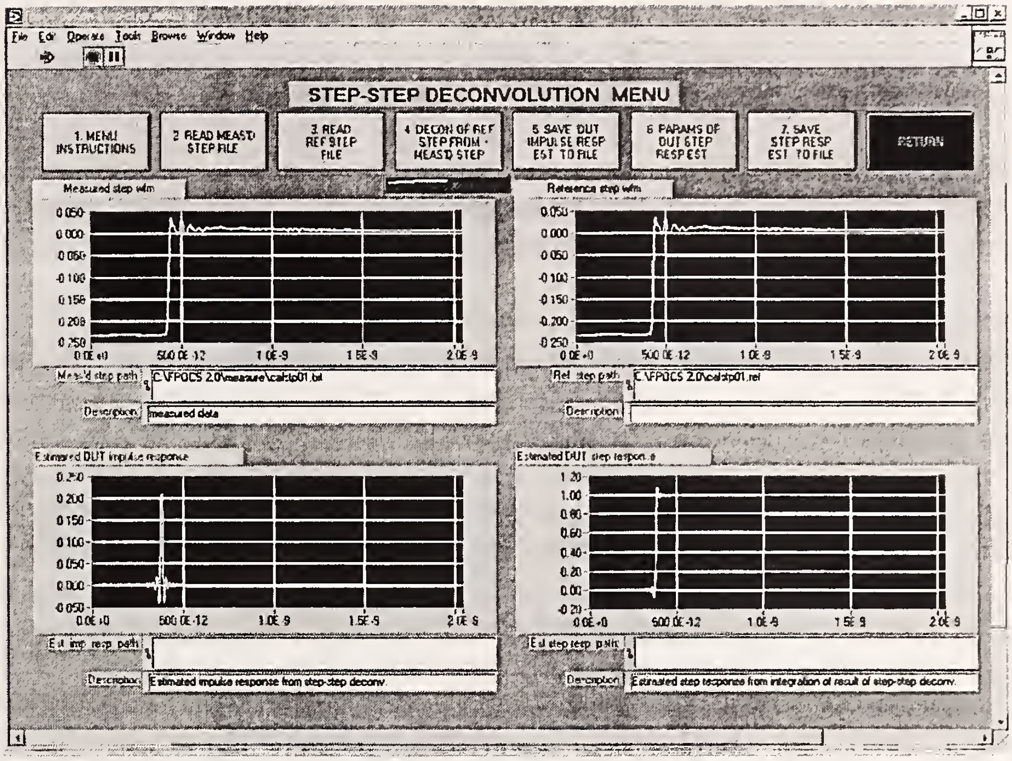

Figure 3-8. FPOCS Step-Step Deconvolution Menu.

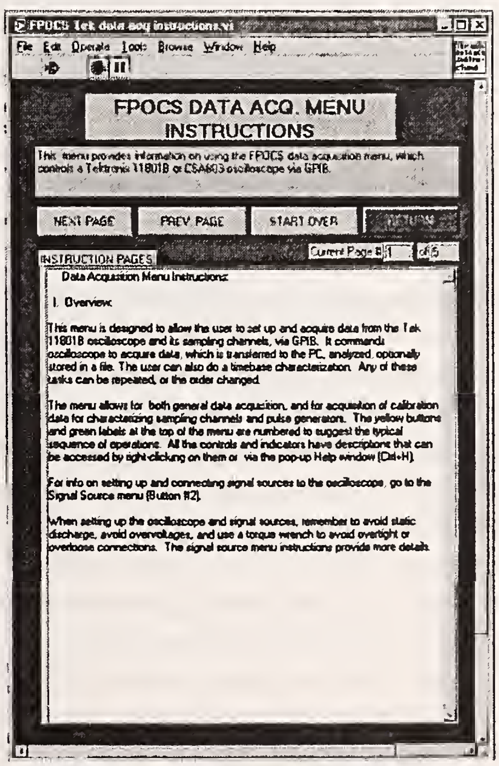

Figure 3-9. Typical FPOCS Instructions/Help Menu.

4. Operating Procedure

The following operating procedures must be strictly followed to obtain consistent, repeatable measurement results.

4.1 Preparation

Prior to beginning the measurements, several records need to be started or updated and the equipment to be used must be prepared for the tests.

4.1.1 Documentation

Once the device to be calibrated has been delivered to the laboratory by the Division Office staff, a manila folder is created as a repository of the test results and all notes on the device under test and test conditions and results, shipping information, etc. This folder is maintained by the group performing the 65200S test and is presently located in a filing cabinet located outside of the shielded room in which the tests are performed. A new test sheet is also prepared and inserted in the three ring binder located near the laboratory entrance, also outside the shielded room. This test sheet is used to maintain a record of the important dates associated with each test which may not be recorded elsewhere, such as the date the device was delivered for testing and the date the test report was finished. It is also used to record the fee charged for the test. The Calibration Services office staff will prepare a blue calibration folder and the Division Office staff will create an entry in the Information System to Support Calibrations (ISSC), a web-based calibration tracking system. Once entered in the ISSC, an email will be sent that contains the due date, the customer purchase order number and the calibration folder number. The ISSC system will also automatically send an email reminder to the individual performing the test when the test due date is one week away. At the same time, the ISSC system will also send an email to the Group Leader of the individual performing the test.

4.1.2 Preparation of Measurement System Components

All connectors are inspected and cleaned prior to connecting the equipment. The connectors are inspected for bent or mis-shapen center or outer conductors. The cleaning procedure is as follows. Blow out the connector with clean, dry compressed gas. Then using a cellular-urethane-foam tipped cleaning swab dipped in an alcohol solution, wipe out the mating surfaces of the connector. Blow out again with clean compressed gas to remove loose particles and excess alcohol. A new swab is used for each connector. The head of the swab should be small enough to fit between the center conductor and the interior of the threaded nut of the connector without applying force to the center conductor. The foam swabs that we are presently using are Chemtronics “Flextips Mini” foam swabs, part number CXM50. It has a 4 mm (3/16 inch) wide, open celled urethane foam head. The alcohol solution that we are using is Radio Shack “Professional Tape Head Cleaner Fluid,” catalog number 44-1113. It is composed of Isopropanol (49 %), Ethanol (48 %), and Methanol (3 %). The clean, dry compressed gas presently used is Chemtronics “Ultra Jet” part number ES1020. The following steps must be performed.

Inspect and clean connectors on DUT.

Inspect and clean connectors on sampler.
Inspect and clean connectors on microwave synthesizer.
Inspect and clean adapter (if any) used between DUT and Sampler.
Inspect and clean connectors on BNC trigger source.
Inspect and clean connectors on the trigger delay line.
Inspect and clean connectors on all cables to be used.
Connect all equipment and cables, using a torque wrench to apply 0.90 Nm to each connection.

Power-on all equipment and let warm-up for at least 2 h before continuing with the test. The two hour time period is not arbitrary, it is a minimum established by monitoring the temperature of the oscilloscope mainframe.

4.2 Data Acquisition

1. Record the temperature and humidity at the beginning of the measurements.

2. Perform Internal Calibration of Sampler Plug-In, found in the Utility menu of the oscilloscope. This sets the vertical gain and offset values.

3. Acquire sinewave data for timebase calibration (use the Gigatronics synthesizer and 100 MHz ref output as the trigger signal to the oscilloscope for best signal to noise). 4.0 GHz and 3.8 GHz are the frequencies that are used most often. At least two frequencies must be used and they must not be harmonically related. At each frequency, at least two phases must be used since the low slope segments of each sinewave are omitted and complete epoch coverage is required. The phase may be adjusting by changing the trigger level a few millivolts.

4. Calculate the timebase error is calculated by running the timebase characterization operation (see Figure 3-6) with the sinewaves just acquired as inputs.

5. Change the trigger source from the Gigatronics synthesizer "100 MHz ref" output to the output of the BNC 6040/201E pulse generator.

6. Examine the timebase error and identify a region of low or zero slope. When measuring the DUT waveforms or when sampling the reference input (kick-out pulse), the transition should be on a low slope region of the timebase error. The transition instant can be positioned by adding a cable or an adapter to the trigger signal path.

7. Acquire DUT waveforms using the FPOCS data acquisition menu. Typical settings are:
   200 ps/div
   transition at 1.5 division (300 ps) from start.
   40 mV/div, -125 mV offset (or as appropriate for the DUT)
   trigger + slope, 2.5 GHz trigger bandwidth, trigger level 280 mV, best throughput setting
   512 averages, 1024 points (4096 points for sampler calibrations)

8. Acquire 3 waveforms, disconnect, re-connect and repeat until at least 12 waveforms acquired.

9. The temperature before and after each waveform is acquired will be automatically logged by the FPOCS Data Acquisition Menu.

10. Measure the jitter by increasing the time resolution to 10 ps/div and using the built-in histogram capabilities of the oscilloscope. A 1.0 mV window should be used for consistent results. Average at least three jitter measurement results.

11. Record the temperature and humidity at the end of the test.

12. Make a record of the test conditions including humidity, temperature, start time and end time, oscilloscope settings, filenames of acquired waveforms, microwave synthesizer settings and trigger generator settings. Also record the use of any adapters and whether or not the customer included a power supply, cable or other items. Note any abnormal or unusual occurrences such as broken parts or unexpected device properties.

4.3 Data Analysis

The pulse parameters are found and tabulated for each acquired waveform using the Waveform Plot and Step Parameters routine in the FPOCS (fig. 3-5) and using the software program "Pulsepar.VI." Each waveform is processed independently of all the others.

The amplitude is found by constructing a histogram of the vertical data. This histogram is then divided into two sub-histograms, an upper and a lower histogram, the division taking place at the mean value of the maximum and minimum waveform values. The modes are found for the upper and lower histograms. The two resulting mode values are taken as the low state (S_1) and high state (S_2), the amplitude being the difference between these two states.

The 10 %, 20 %, 50 %, 80 %, and 90 % reference levels are then calculated using the waveform amplitude just found. The reference level instants (instant that the waveform intersects the reference level) are then found for each reference level. Since the discrete waveform values often do not occur at the sought reference level, linear interpolation of the data is used. The 10 % to 90 % transition duration is the difference between the 10 % and 90 % reference level instants. The 20 % to 80 % transition duration is defined similarly.

The acquired waveforms are processed to remove the effects of the finite bandwidth of the sampler. The deconvolution of sampler impulse response is done using the routine in the FPOCS and latest sampler impulse response estimate. The deconvolution algorithm is described in reference [25] and was developed by Tamas Daboczi while a guest researcher at NIST. The deconvolved waveforms are also stored on the computer.

The pulse parameters for these deconvolved waveforms are found as previously described.

4.4 Preparation of the Uncertainty Analysis
The uncertainty analysis has been automated using LabVIEW VIs. Update the Jitter Control Chart, the Gain Control Chart (if applicable), and the Temperature data in the Uncertainty VIs. A listing file for the acquired data and another for the deconvolved data is also created. Calculate the uncertainty using the LabVIEW Uncertainty VIs for Amplitude and Transition Duration. Print the front panel for each parameter's uncertainty.

4.5 Preparation of the Report Of Special Test
The values reported are: amplitude, transition duration (both 10 % to 90 % and 20 % to 80 % transition durations), undershoot and overshoot. The reported amplitude value is the average of all acquired waveforms amplitudes. The transition duration, undershoot and overshoot parameter values are the average of the respective parameters of all the deconvolved waveforms.

The Report of Special Test is generated by retrieving the last test report and changing the entries as needed. The assigned folder number, customer name, device serial number, and list of test conditions and notes need particular attention in the updating process.

Example waveforms are also included in the report. Select an acquired waveform with a transition duration closest to the reported, average transition duration for inclusion in the Report of Special Test. Also select a deconvolved waveform using the same criteria for inclusion. Presently, the AXUM graphing software package is used for plotting the waveform data and importing into the Report. An example of the Report of Special Test is found in Appendix A1.

Clean the connectors of the DUT and repack in shipping container provided by the customer.

In addition to the Report of Special Test, an attachment outlining the uncertainty analysis and measurement system has been prepared and is provided to the customer.

4.6 Miscellaneous Tasks
After the report is finished and signed, it must be reviewed by the Project Leader, Group Leader and Division Chief. The Project Leader must initial the "Check Copy" of the Report which will be archived by the Division Office staff. Two copies (the Check Copy and Customers Copy) should be placed in the blue calibration folder (prepared and delivered by Division Office staff) along with the attachment. A third copy is filed with the test notes in the manila folder prepared at the beginning of the test.

The blue folder also contains the return shipping documents and information. These should be placed with the device, and left on the work surface near the door to the hallway for pickup by the Division Office personnel. They will arrange return of the device to the customer.

The ISSC must be notified that the calibration is complete or it will automatically send email messages to the operator and his supervisors when the calibration estimated completion date nears. The operator of this service must visit the ISSC web site at: http://www-i.nist.gov/calbin/calibration.cgi, enter the “Technical Staff Functions” (username and password required) and “Close Test and Enter Calibration Data.” The only function currently being used by this service is the calibration date; no reports are generated or fees calculated.

5. Uncertainty Analysis

The uncertainty analysis follows NIST recommended practice as outlined in [28]. Originally, both Type A and B uncertainties were identified. After extensive measurement system characterization, most Type B uncertainties have been replaced by Type A. In many cases, this resulted in a reduction in reported uncertainty. The following section outlines the uncertainty analysis associated with each reported parameter; for more detail, see Appendix A2.

5.1 Pulse Amplitude Uncertainty

Calculating the uncertainty in the pulse amplitude requires having an equation that describes the reported pulse amplitude, $V_{A,}$. For our system:

$$V_A = \frac{\overline{V_{A,c} + V_{\Delta T}}}{\overline{g}} = \left(\overline{V}_{A,c} + \overline{V}_{\Delta T}\right)/\overline{g}, \tag{6}$$

where the horizontal bars represent the arithmetic mean, $\overline{V}_{A,c}$ is the average of the set of M_1 pulse amplitudes corrected for sampler offset errors, $\overline{V}_{\Delta T}$ is the average of the amplitude corrections required for a change in measurement temperature, and $\overline{g}$ is the transient gain correction of the sampler. Ideally, $\overline{g} = 1$ if the sampler exhibits no pulse gain or attenuation and the sampler has settled within the waveform epoch. The $\overline{V}_{A,c}$ is given by:

$$\begin{aligned} \overline{V}_{A,c} &= \overline{V}_{S2,c} - \overline{V}_{S1,c} \\ &= \overline{V}_{S2,m} - \overline{V}_{S2,off,m} - \left(\overline{V}_{S1,m} - \overline{V}_{S1,off,m}\right), \end{aligned} \tag{7}$$

where $\overline{V}_{off}$ is the voltage offset. The "c" and "m" in the subscripts refer to corrected and measured voltage values. We have observed that for the presently-available, high-bandwidth samplers, the voltage offset error is the same for both the top line (S2) and bottom line (S1) voltage levels, therefore, the offset voltage contribution can be ignored since it is zero.
The temperature correction term is obtained by measuring the change in the observed pulse amplitude with temperature (see Fig. 5-1) [29] and is given by:

$$\overline{V}_{\Delta T} = S_{\Delta V/\Delta T}\left(\overline{T}_{meas} - \overline{T}_{ref}\right), \tag{8}$$

where $\overline{T}_{meas}$ is the average of M_T temperature values taken during the pulse measurement process, S is the slope of a straight line fit through a set of previously-acquired amplitude versus temperature data, and $\overline{T}_{ref}$ is the average temperature of the sampling head taken when the sampler impulse response was determined.

The transient gain term, $\overline{g}$, is obtained by taking the ratio of the amplitude of the reference pulse as measured using the sampler and the amplitude of the reference pulse as measured using the SWA reference instrument. As mentioned earlier, the gain term is obtained from a control chart and is given by:

$$\overline{g} = \frac{1}{M_g}\sum_{i=1}^{M_g} g_i = \frac{1}{M_g}\sum_{i=1}^{M_g}\frac{\overline{V}_{S2,m,r,i} - \overline{V}_{S1,m,r,i}}{\overline{V}_{S2,r,r,i} - \overline{V}_{S1,r,r,i}}, \tag{9}$$

where the "r,r" in the subscript denotes the reference measurement instrument with reference pulse generator, "m,r" denotes test instrument and reference pulse generator, and there are M_g independent gain measurements.

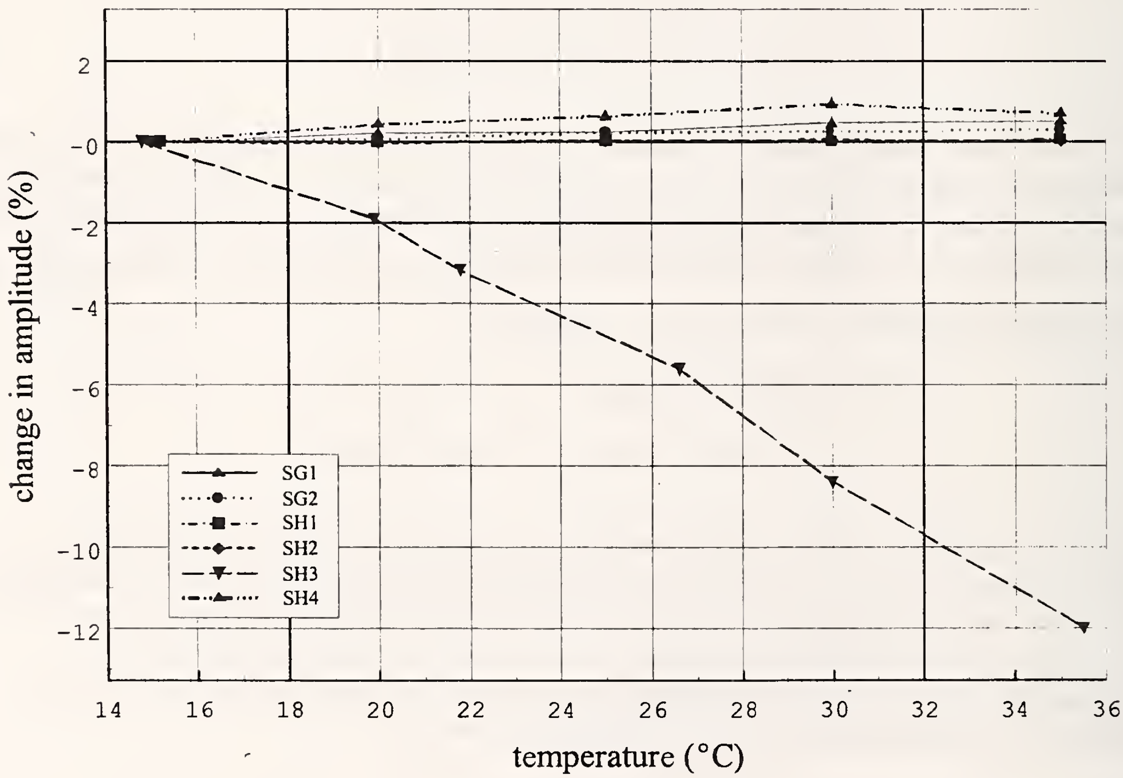

Figure 5-1. The percent change in pulse amplitude with temperature relative to 15 °C.

In addition to measurement-related uncertainties, the reported amplitude values are also subject to uncertainties from the method used to calculate these values, which in this case, is a histogram method. The histogram-derived amplitude values, for example for V_{S2}, are given by:

$$V_{S2} = N_{S2}\frac{V_{max} - V_{min}}{N_{bins}} + V_{min}, \tag{10}$$

where N_{bins} is the number of histogram bins and N_{S2} is the bin number of the topline mode bin in the histogram.

Each of these variables contribute to the pulse amplitude. To determine the uncertainty in the estimate of the pulse amplitude, the partial derivatives of equations 6-10 are taken with respect to the appropriate variables. These partial derivatives are listed in Tables 1a-1c in Appendix A2, "Pulse Parameter Uncertainty Analysis," Metrologia, Vol. 39, pp143-155, 2002. As previously stated, the calculation of the uncertainty has been automated using a LabVIEW VI. The Uncertainty, Amplitude VI determines the value of each of these partial derivatives and combines them in quadrature [28]. The coverage factors are calculated and the expanded uncertainty with 95 % confidence bounds is calculated and reported with the estimate of the pulse amplitude.

5.2 Transition Duration Uncertainty

The reported (and therefore, reconstructed) waveform transition duration, t_d, is the average transition duration extracted from M_1 reconstructed pulse waveforms. The t_d is related to the transition duration of the measured waveform, $t_{d,m}$, and the transition duration of the sampler step response, $t_{d,r}$:

$$t_d = \frac{\sum_{i=1}^{M_1} t_{d,R,i}}{} = f_{dec}\left(t_{d,m}, t_{d,r}\right) + \Delta t_{d,\Delta T}, \tag{11}$$

where T is temperature and $t_{d,R}$, $t_{d,m}$, and $t_{d,r}$ are the transition durations of the reconstructed, measured, and sampler step response waveforms. The specific deconvolution functional relationship, f_{dec}, between t_d, $t_{d,m}$, and $t_{d,r}$ is dependent on the type of waveforms used. For example, for a Gaussian waveform, t_d is equal to the square root of the difference of the squares of transition durations of the measured and step response waveforms. The $\Delta t_{d,\Delta T}$ is the temperature-induced incremental change in transition duration [29].

Since we do not know a priori the functional relationship between t_d, $t_{d,m}$, and $t_{d,r}$, we obtain an empirical relationship for the three parameters. We obtain this relationship by fitting a curve (such as a polynomial) to $t_{d,R}$ versus $t_{d,m}$ data and separately to $t_{d,R}$ versus $t_{d,r}$ data where both $t_{d,m}$ and $t_{d,r}$ are varied within expected values and the t_d is obtained from the reconstructed waveforms. The $t_{d,m}$ and $t_{d,r}$ can be put in terms of the sampling intervals:

$$\begin{aligned} t_{d,m} &= X_m \delta t, \\ t_{d,r} &= X_{rj} \delta t, \end{aligned} \tag{12}$$

where X_m and X_{rj} are the real-valued (non-integer) number of sampling intervals describing the transition duration for the measured sampler step response waveforms (which includes jitter) and δt is the duration of the equi-spaced sampling interval. The δt is the average duration of the sampling interval over the waveform epoch [30] and is measured using sine-fit techniques [22] during the timebase error measurement process. Figure 5-2 shows the timebase errors taken from two different sampling oscilloscopes. X_{rj} is the result of the convolution of the measurement jitter and the sampler step response:

$$X_{rj} = \sqrt{X_r^2 + X_j^2}, \tag{13}$$

where X_r and X_j are the number of sampling intervals in the sampler step response and equivalent

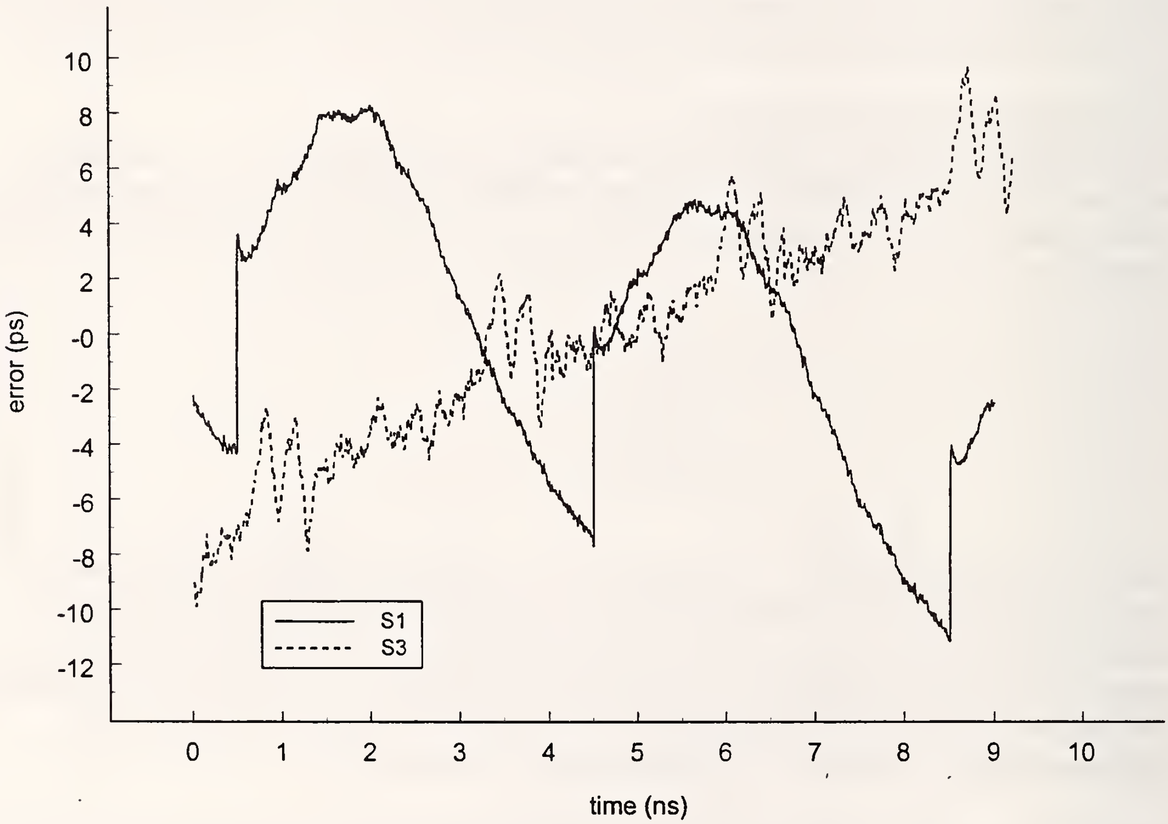

Figure 5-2. Timebase errors.

jitter step response transition durations. Although X_r may not accurately be described by a Gaussian waveform, X_r and X_j are added in quadrature (Gaussian approximation) to get X_{rj}. Errors are associated with this approximation [31,32] and the uncertainty bounds are adjusted accordingly. The X_j includes drift of the sampling aperture with respect to its trigger. The temperature dependent change in transition duration can be expanded:

$$\Delta t_{d,\Delta T} = S_{\Delta t/\Delta T}\left(\overline{T}_{meas} - \overline{T}_{ref}\right). \tag{14}$$

The curve, $S_{\Delta t/\Delta T}$, is a straight line fit to the M_S measured transition duration versus temperature data pairs that are measured independently of the M_l acquired waveforms. Using (12) and (14) in (11) gives:

$$t_d = \overline{f_{dec}(X_m, X_{rj})}\delta t + S_{\Delta t/\Delta T}\left(\overline{T}_{meas} - \overline{T}_{ref}\right). \qquad (15)$$

For samplers and pulse generators presently in use at NIST, the value of $S_{\Delta t/\Delta T}$ is approximately zero or is much less than the reported uncertainties, however, it will be maintained here for completeness.

The values of X_m, X_r, and X_j are determined by linear interpolation to obtain the instant in time (the reference level instant) corresponding to the given reference level. The value of X_m (and analogously for X_r and X_j), is:

$$X_m = \frac{t_{L2} - t_{L1}}{\delta t}, \qquad (16)$$

where t_{L1} and t_{L2} are the time instances corresponding to the first (L1) and second (L2) reference levels of the transition duration. For example, in the 10 % to 90 % transition duration, L1 is the 10 % reference level instant and L2 is the 90 % reference level instant. The t_{L1} is given by:

$$t_{L1} = t_{L1-} + \frac{t_{L1+} - t_{L1-}}{L1_+ - L1_-}\left(L1 - L1_-\right), \qquad (17)$$

where the "+" and "-" subscripts denote the actual data values found immediately above and below the reference level and, for the time variables, the subscripts correspond to sampling instances of the those data. The t_{L2} can be expanded similarly to that done for t_{L2}. The values of L1 and L2 can be expanded:

$$\begin{aligned} L1 &= V_{S1,m} + P1(V_{S2,m} - V_{S1,m}), \\ L2 &= V_{S1,m} + P2(V_{S2,m} - V_{S1,m}), \end{aligned} \qquad (18)$$

where P1 and P2 are the percent reference values, such as 10 % and 90 % or 20 % and 80 %.

Each of these variables contribute to the transition duration. To determine the uncertainty in the estimate of the transition duration, the partial derivatives of Equations 11-18 are taken with respect to the appropriate variables. These partial derivatives are listed in Tables 2a-2d in Appendix A2. The calculation of the uncertainty has been automated using a LabVIEW VI. The Uncertainty, Transition Duration VI determines the value of each of these partial derivatives and combines them in quadrature [28]. The coverage factors are calculated and the expanded uncertainty with 95 % confidence bounds is calculated and reported with the estimate of the transition duration.

5.3 Overshoot Uncertainty

Voltage offset errors will not be considered here because they will cancel as they did for the uncertainty calculation of $V_{A,c}$. The equation describing the calculation for the overshoot is:

$$OS = \overline{\left(\frac{V_{max,R} - V_{S2,R}}{V_{A,R}} \right)}. \tag{19}$$

where $V_{max,R}$ is the maximum voltage in the appropriate aberration region of the reconstructed waveform, $V_{S2,R}$ is the voltage corresponding to State 2 of the reconstructed waveform and $V_{A,R}$ is the amplitude of the reconstructed waveform. Overshoot is usually presented as a percentage. $V_{max,R}$ can be written as:

$$V_{max,R} = V_{S2,R} + V_{OS,R}, \tag{20}$$

where

$$V_{OS,R} = \frac{b_{OS} V_{OS,m} t_{d,m}}{t_{d,R}}, \tag{21}$$

and β_{OS} is a correction factor that is determined experimentally and $V_{OS,m}$ is the overshoot of the acquired waveform. Equation (21) describes an empirical relationship between the overshoot and transition duration of the reconstructed (reported) waveform and that of the measured waveform. In (21), we assume that the product of the overshoot voltage and transition duration is not affected by an all-pass filter, which is how the sampler impulse response is expected to behave for an input signal that has a bandwidth lower than that of the sampler. $V_{OS,m}$ can be expanded:

$$V_{OS,m} = V_{max,m} - V_{S2,m}. \tag{22}$$

The $t_{d,R}$ can be expanded similar to that of $t_{d,m}$, and using this expansion and (12), (20), (21), and (22) in (19) yields for OS:

$$OS = \overline{\left(\frac{1}{V_{S2,R} - V_{S1,R}} \right) \left(V_{S2,m} + \beta_{OS} \left[V_{max,m} - V_{S2,m} \right] \frac{X_m}{X_R} - V_{S2,R} \right)}, \tag{23}$$

where X_R is the real-valued number of sampling intervals describing the transition duration of the reconstructed waveform. The correction factor β_{OS} is determined by fitting a curve to a set of M_9 $t_{d,m}V_{OS,m}$ versus $t_{d,R}V_{OS,R}$ data. The $t_{d,m}$ and $V_{OS,m}$ are obtained from the acquired waveforms and the $t_{d,R}$ and $V_{OS,R}$ parameters are obtained from the reconstructed waveforms. The uncertainty in β_{OS} is the standard deviation in the fitted curve relative to the set of corresponding $t_{d,m}V_{OS,m}$ versus $t_{d,R}V_{OS,R}$ data, and the coverage factor is determined by the number of β_{OS}s.

Equation 23 identifies the variables that contribute to the overshoot. To determine the uncertainty in the estimate of the overshoot, the partial derivative of equation 23 is taken with respect to each of these variables. These partial derivatives are listed in Table 3 that appears in Appendix A2. The calculation of the uncertainty has been automated using a LabVIEW VI. The Uncertainty, Overshoot VI determines the value of each of these partial derivatives and combines them in quadrature [28]. The coverage factors are calculated and the expanded uncertainty with 95 % confidence bounds is calculated and reported with the estimate of the overshoot.

5.4 Undershoot (preshoot) Uncertainty

The undershoot uncertainty calculation is performed similarly to the overshoot uncertainty calculation (see Sec. 5.3) with the appropriate change in variables. This uncertainty estimate yields:

$$US = \overline{\left(\frac{1}{V_{S2,R} - V_{S1,R}}\right)\left(V_{S1,m} + \beta_{US}\left[V_{min,m} - V_{S1,m}\right]\frac{X_m}{X_R} - V_{S1,R}\right)}, \quad (24)$$

where β_{US} is a correction factor that is determined experimentally as is done for β_{OS}. Equation (20) provides an empirical relationship between the undershoot and transition duration of the reconstructed (reported) waveform and that of the measured waveform. The correction factor β_{US} is determined by fitting a curve to a set of M_9 $t_{d,R}V_{US,R}$ versus $t_{d,m}V_{US,m}$ data. The uncertainty in β_{US} is the standard deviation in the fitted curve relative to the set of corresponding $t_{d,m}V_{US,m}$ versus $t_{d,R}V_{US,R}$ data, and the coverage factor is determined by the number of β_{US}s.

Equation 24 identifies the variables that contribute to the undershoot. To determine the uncertainty in the estimate of the undershoot, the partial derivative of Equation 23 is taken with respect to each of these variables. These partial derivatives are listed in Table 4 that appears in Appendix A2. The calculation of the uncertainty has been automated using a LabVIEW VI. The Uncertainty, Undershoot VI determines the value of each of these partial derivatives and combines them in quadrature [28]. The coverage factors are calculated and the expanded uncertainty with 95 % confidence bounds is calculated and reported with the estimate of the undershoot.

6. Procedures for Quality Control

The quality of the measurement service has benefitted from having just one person responsible for the measurements for many years. The previous operators of the service have been conscientious and skilled. Other quality control measures are incorporated in the service.

6.1 Control Charts

Several control charts are maintained as part of the service. These are used in the uncertainty analysis and any significant change will negatively impact (increase) the uncertainty of the measurement results. The impulse response estimate is obtained using the Nose-to-Nose technique and is done periodically. This estimate is added to a Impulse Response Control Chart and compared to previous estimates. The single most important piece of equipment is the sampler and its condition is indicated by the impulse response estimate. A change in the gain of the sampler would also indicate a degradation of the sampler and the Gain Control Chart is monitored for changes.

6.2 Check Standard

No check standards are maintained by this service, however, as part of each calibration, the transition duration and amplitude estimate is compared with prior estimates obtained for that particular device. The DUT then become a "check standard." If the new estimate is outside the uncertainty bounds of the prior estimate, then an attempt is made to identify the problem. If the conclusion is that the DUT has changed, the customer is notified.

6.3 Procedure to Amend a Calibration

If an error is found in a calibration report that has already been delivered to the customer, the Project Leader is notified. After discussing the error and possible routes to correct the error, a proposed route is brought to the Group Leader. The Group Leader approves the correction.

7. References

1. N.G. Paulter and D.R. Larson, "NIST's High-Speed Pulse Parameter Measurement Service," IEEE Instrumentation and Measurement Technology Conference, Anchorage, AK, USA 21-23, May 2002.
2. IEEE Standard 181-2003.
3. Pulse Techniques and Apparatus, Part 1: Pulse Terms and Definitions; Part 2: Pulse Measurements and Analysis, General Considerations, IEC Publications 469-1 and 469-2, Intl. Electrotech. Com. (IEC), Switzerland (1974).
4. S.M. Sze, Physics of Semiconductor Devices, Second Edition, John Wiley & Sons, New York, 1981.
5. B.G. Streetman, Solid State Electronic Devices, Second Edition, Prentice Hall, Inc., Englewood Cliffs, NJ, 1980.
6. C. Hamilton, D. McDonald, J. Sauvageau, and S. Whiteley, "Standards and High-Speed Instrumentation," Proc. IEEE, Vol. 77, pp. 1224-1232, 1989.
7. A. Yariv and P. Yeh, Optical Waves in Crystals, Propagation and Control of Laser Radiation, John Wiley & Sons, New York, 1984.
8. D.H. Auston and M.C. Nuss, "Electrooptic generation and detection of femtosecond electrical transients," IEEE J. Quantum Electronics, Vol. 24, pp. 184-197, 1988.
9. J.A. Valdmanis and G. Mourou, "Subpicosecond electrooptic sampling: Principles and applications," IEEE J. Quantum Electronics, Vol QE-22, pp. 69-78, 1986.
10. B.H. Kolner and D.M. Bloom, "Subpicosecond electroopic sampling in GaAs integrated circuits," IEEE J. Quantum Electronics, Vol. QE-22, pp. 79-93, 1986.
11. D. Henderson, A.G. Roddie, and A.J.A. Smith, "Recent developments in the calibration of fast sampling oscilloscopes," IEE Proceedings-A, Vol. 139, pp. 254-260, September 1992.
12. D.H. Auston, "Picosecond optoelectronic switching and gating in silicon," Appl. Phys. Lett., vol. 26, pp. 101-103, 1975.
13. F.J. Leonberger and P.F. Moulton, "High-speed InP optoelectronic switch," Appl. Phys. Lett., vol. 35, pp. 712-714, 1979.
14. G. Mourou and W. Knox, "High-power switching with picosecond precision," Appl. Phys. Lett., vol. 35, pp. 492-495, 1979.
15. R.B. Hammond, N.G. Paulter, A.E. Iverson, and R.C. Smith, "Sub-100 ps bulk-recombination-limited InP:Fe photoconductive detector," pp. 157-160, IEEE Int. Electron Devices Meet. Tech. Dig., 1981.
16. N.G. Paulter, "Selecting a short-pulse laser system for photoconductive generation of high-speed electrical pulses," Optical Engineering, Vol. 35, pp. 3296-3300, November 1996.
17. D.E. Cooper and S.C. Moss, "Picosecond optoelectronic measurement of the high-frequency scattering parameters of a GaAs FET," IEEE J. Quantum Electronics, Vol. QE-22, pp. 94-100, 1986.
18. N.G. Paulter, High-speed optoelectronic pulse generation and sampling system," IEEE Trans. Instrum. Meas., Vol. 37, pp. 449-453, September 1988.

19. S.M. Riad, "Modeling of the HP-1430A feedthrough wideband (28 ps) sampling head," IEEE Trans. Instrum. Meas., Vol. 31, pp. 110-115, June 1982.
20. K. Rush, S. Draving, and J. Kerley, "Characterizing high-speed oscilloscopes," IEEE Spectrum, pp. 38-39, September 1990.
21. J. Verspecht, "Broadband sampling oscilloscope characterization with the 'nose-to-nose' calibration procedure: A theoretical and practical analysis," IEEE Trans. Instrum. Meas., Vol. 44, pp. 991-997, December 1995.
22. G.N. Stenbakken and J.P. Deyst, "Time-base nonlinearity determination using iterated sine-fit analysis," IEEE Trans. Instrum. Meas., Vol. 47, pp. 1056-1061, October 1998.
23. T.M. Souders, B.C. Waltrip, O.B. Laug, and J.P. Deyst, "A wideband sampling voltmeter," IEEE Trans. Instrum. Meas., Vol. 46, pp. 947-953, August 1997.
24. P.S. Filipski, C.J. van Mullen, D. Janik, M. Klonz, J.R. Kinard, T.E. Lipe, and B.C. Waltrip, "Comparison of high-frequency ac-dc voltage transfer standards at NRC, VSL, PTB, and NIST," IEEE Trans. Instrum. Meas., Vol. 50, pp. 349-352, April 2001.
25. T. Dabózi and I. Kollár, "Multiparameter optimization of inverse filtering algorithms," IEEE Trans. Instrum. Meas., Vol. 45, pp. 417 to 421, April 1996.
26. N.S. Nahman and M.E. Guillaume, "Deconvolution of time domain waveforms in the presence of noise," National Bureau of Standards Technical Note 1047, U.S. Department of Commerce, Washington, DC, 1981.
27. N.G. Paulter, "A causal regularizing deconvolution filter for optimal waveform reconstruction," IEEE Trans. Instrum. Meas., Vol. 43, pp. 740-747, October 1994.
28. B.N. Taylor and C.E. Kuyatt, NIST Technical Note 1297, "Guidelines for evaluating and expressing the uncertainty of NIST measurement results," U.S. Dept. Commerce, 1994.
29. D.R. Larson and N.G. Paulter, "Temperature effects on the high-speed response of digitizing sampling oscilloscopes," NCSL International, 2000 Workshop and Symposium, Toronto, Canada, 16-20 July 2000.
30. N.G. Paulter and D.R. Larson, "Time-base setting dependence of pulse parameters using high-bandwidth digital sampling oscilloscope," NCSL International, 2000 Workshop and Symposium, Toronto, Canada, 16-20 July 2000.
31. C. Mittermayer and A. Steininger, "On the determination of dynamic errors for rise time measurement with an oscilloscope," IEEE Trans. Instrum. Meas., Vol. 48, December 1999, pp. 1103-1107.
32. W.L. Gans, "The measurement and deconvolution of time jitter in equivalent-time waveform samplers," IEEE Trans. Instrum. Meas., Vol. IM-32, pp. 126-133, March 1983.

Other Applicable Documents

33. Dynamic Calibration of Waveform Recorders and Oscilloscopes Using Pulse Standards, W. L. Gans, IEEE Trans. Instrum. Meas, Vol. 39 (6), pp. 952- 957 (Dec. 1990).
34. D.R. Larson and N.G. Paulter, "The effect of offset voltage on the kick-out pulses used in the nose-to-nose sampler impulse response characterization method," Instrumentation and Measurement Technology Conference, IMTC 2000, Baltimore, USA, pp. 1425-1428, 1-4 May 2000.

Appendices

A1. Sample Report of Special Test.

A2. N.G. Paulter and D.R. Larson, "Pulse Parameter Uncertainty Analysis," Metrologia, Vol. 39, pp. 143-155, 2002.

REPORT OF SPECIAL TEST

Special Test No. 65200S: Fast Repetitive Pulse Parameters

PULSE GENERATOR HEAD
Manufacturer
Model number, Serial number

Submitted by:

Customer
Somewhere, Worldwide

The pulse amplitude and the pulse first transition durations (both the 20 % to 80 % and 10 % to 90 % definitions) were measured using the NIST Waveform Parameter Analysis System (WPAS). The results are presented in Table 1. The expanded uncertainty bounds shown correspond to a 95 % level of confidence. (See Attachment for further details.)

TABLE 1

Pulse Amplitude	245.3 mV ± 1.5 mV
Pulse First Transition Duration (20 % to 80 %)	10.5 ps ±1.25 ps
Pulse First Transition Duration (10 % to 90 %)	15.6 ps ±1.25 ps

Pulse Generator Head
manufacturer.
Model number, serial number

Test Conditions and Notes for this Special Test

1. The pulse generator head was received on January 27, 2004 in good condition. No power supply was shipped with the subject pulse generator, NIST provided the necessary power supply.
2. Laboratory ambient temperature = 22.6 °C ± 1.0 °C.
3. Laboratory ambient relative humidity = 19 % ± 10 %.
4. The APC-3.5 male output connector of the subject pulse generator head was connected to a precision APC-3.5 to APC-2.4 connector adapter. This was connected to the APC-2.4 connector of the sampler. The necessary trigger pulse for the subject pulse generator head was furnished by a NIST-supplied rectangular pulse generator. The trigger pulse amplitude was 1.0 V (0.0 V low state, 1.0 V high state) and the repetition rate was 100.0 kHz. The equipment was allowed to operate for at least two hours prior to measurement.
5. The oscilloscope trigger delay was adjusted to place the 50 % pulse amplitude reference level instant of the first transition approximately 300 ps from the start of the 2.0 ns pulse waveform epoch.
6. Figure 1 is a plot of one of the subject pulse generator waveforms as acquired with the WPAS. This plot shows the pulse waveform before any corrections for voltage-axis and time-axis gain and linearity, jitter deconvolution when necessary, and deconvolution of the sampler impulse response. Figure 2 is a plot of the waveform after the necessary corrections have been made.

For the Director,
National Institute of Standards
and Technology

Gerald FitzPatrick, Group Leader
Quantum Electrical Metrology Division

Special Test performed by:

Donald R. Larson
(301) 975-2437

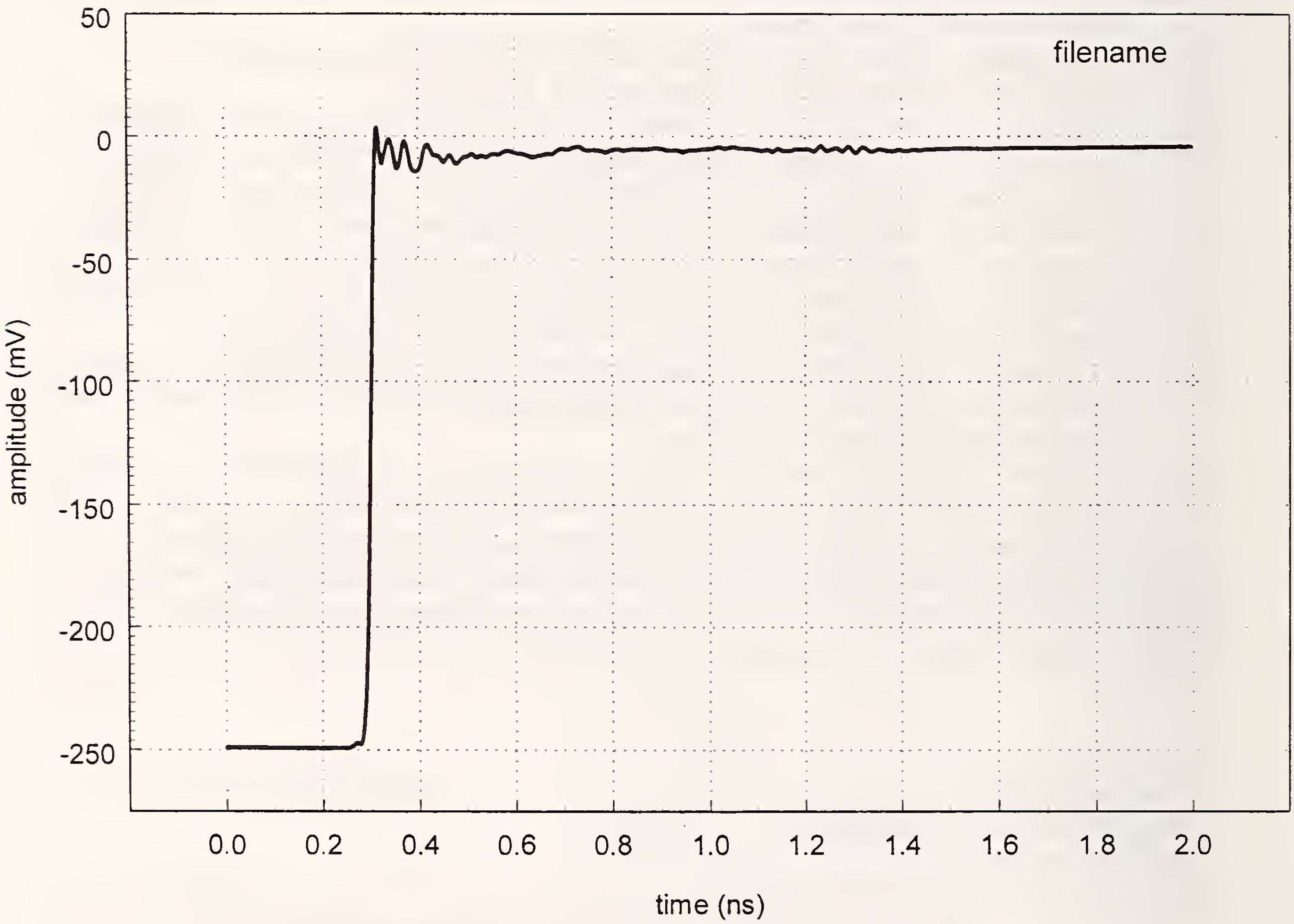

Figure 1. Measured waveform, Customer, Manufacturer, model number, serial number.

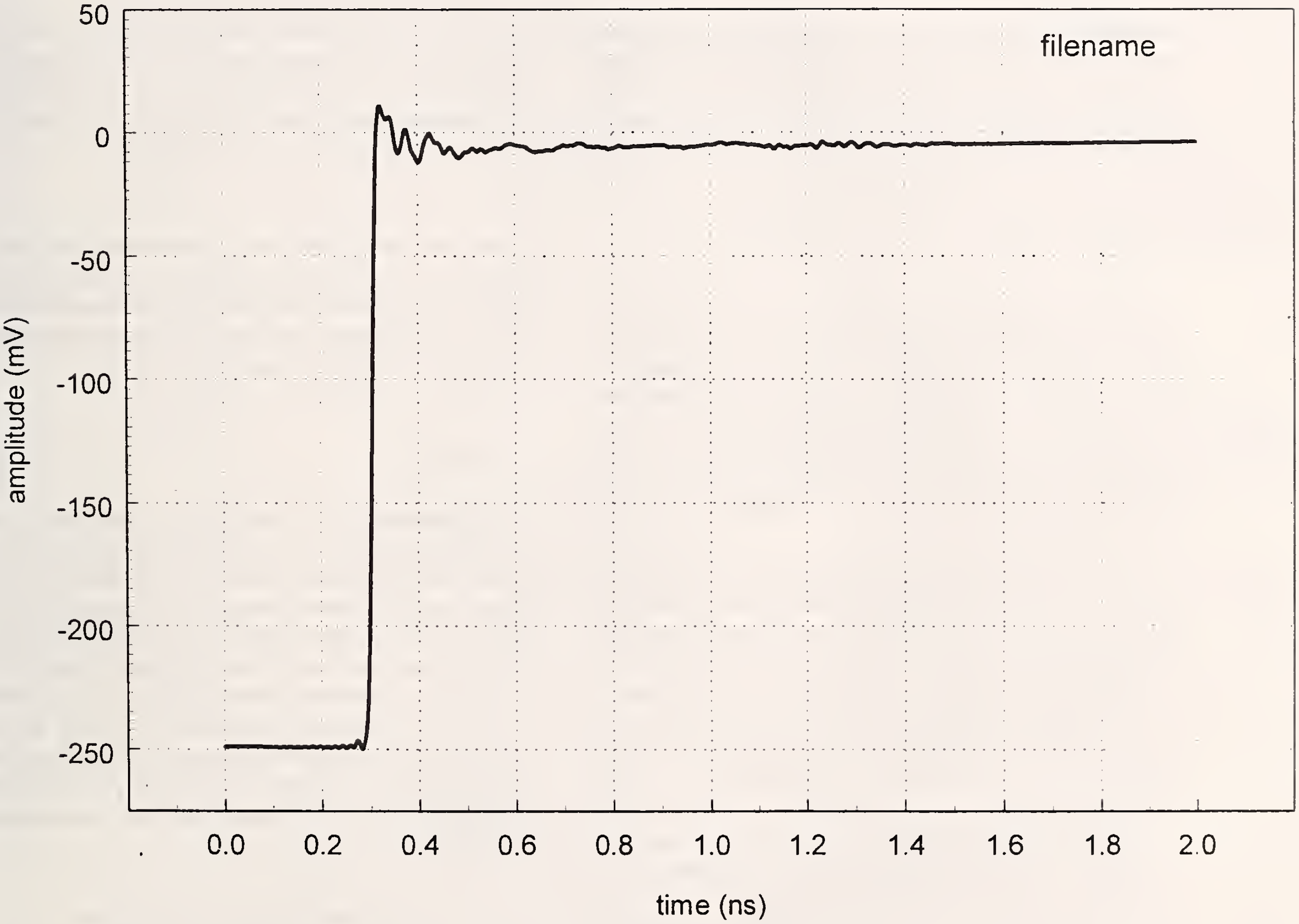

Figure 2. Deconvolved waveform, Customer, Manufacturer, model number, serial number.

Pulse parameter uncertainty analysis

N. G. Paulter and D. R. Larson

Abstract. A detailed uncertainty analysis is presented for the pulse parameter measurement service of the National Institute of Standards and Technology (NIST, USA). It relates to the new pulse parameter measurement and extraction processes. Uncertainties for pulse amplitude, transition duration, overshoot and undershoot (preshoot) are given. Effects of temperature variation, impulse response estimate, pulse parameter extraction algorithms, time-base distortion, calibration procedures and the waveform reconstruction process are included.

1. Introduction

The NIST supports a measurement service for high-speed (transition durations <20 ps) pulse generators that provides an estimate of the pulse parameters of amplitude and transition duration [1]. Overshoot and undershoot (preshoot) parameters were previously provided as well. However, support for these parameters was discontinued because of the lack of a viable uncertainty analysis [2], which is addressed by this paper.

The NIST is one of two national laboratories that provide a pulse parameter measurement service; the other being the National Physical Laboratory (NPL) in the United Kingdom. The NIST and NPL are performing a comparison of pulse parameter results, which includes measured data, corrected data (if applicable) and reconstructed data. The results to date indicate that both national laboratories are in close agreement.

The NIST measurement service currently uses commercial, high-bandwidth sampling oscilloscopes (3 dB attenuation, bandwidths of approximately 50 GHz) and pulse generators (3 dB attenuation, bandwidths of approximately 20 GHz) to measure the pulse parameters of short-transition-duration (high-speed) pulse generators and the step response of high-speed samplers. The purpose of this paper is to present our new uncertainty analysis for these parameters, which are pulse amplitude, transition duration, overshoot and undershoot.

For brevity, not all variables are described at the point of first use, but a list of variables and their description is provided in the glossary. Also, it should be pointed out that the step response of a device is equal to the convolution integral of the impulse response of that device with an ideal step. Both terms are used in this paper because transition durations and bandwidths of electronic systems are typically calculated from the step responses and, in waveform reconstruction, impulse responses are typically deconvolved.

2. Background

The pulse parameter measurement process that is used to acquire waveforms is briefly described in this section. The measurement process consists of a set of measurements of the customer's pulse generator or sampler (the device under test, or DUT) and a set of instrument calibration measurements. Some of the instrument calibration measurements are made during the DUT measurement sequence and some are not. The calibration measurements include time-base errors, sampler gain, jitter and sampler step response. Figure 1 is a diagram of the NIST pulse parameter measurement system.

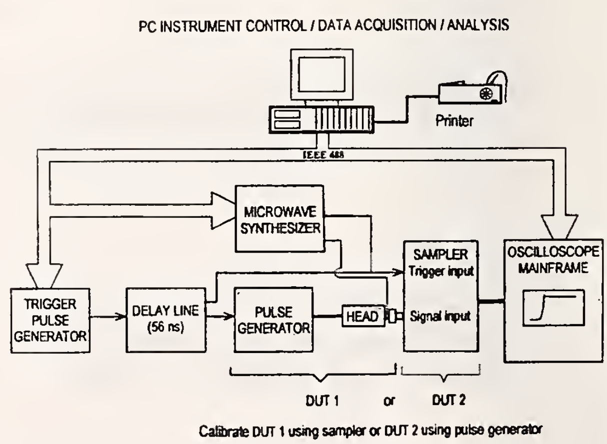

Figure 1. Diagram of NIST pulse measurement system. The dotted lines indicate insertion of instruments used in time-base calibration.

N. G. Paulter and D. R. Larson: Electricity Division, National Institute of Standards and Technology (NIST), 100 Bureau Drive, Gaithersburg, MD 20899, USA.

An estimate of the step response of the NIST 50 GHz sampler used to measure the DUT is obtained using the "nose-to-nose" method [3, 4], the results of which have been compared with results using swept frequency and optoelectronic methods [5]. We are currently examining the "nose-to-nose" method and its limitation in sampler calibration [6]. Measurements that are used to estimate the sampler step response, system jitter and dynamic gain of the sampler are taken routinely, but not necessarily as part of the DUT measurement sequence, and a control chart is maintained for the mean value and standard deviation of the transition durations of the sampler step response and the equivalent jitter step response and the sampler dynamic gain. The reason that the measurements of these parameters are not part of the DUT measurement sequence is that the sampler step response, the system jitter and the sampler dynamic gain are stable (small observable variation) and the variations in these parameters are represented in their associated control chart data. The DUT jitter is intentionally excluded from the system jitter because DUT jitter affects the DUT parameters of transition duration, overshoot and undershoot and will be exhibited in customer measurements.

Several sets of data are acquired for the customer's DUT. For brevity, the discussion that follows assumes that the DUT is a pulse generator. A set of data consists of M_1 sampler-acquired DUT waveforms and one measurement of the time-base errors. Measurements of the time-base errors [7-10] are a routine part of the DUT measurement procedure. The DUT measurement sequence is as follows:

1. measure time-base error: one independent measurement;
2. acquire waveforms: M_1 independent measurements of DUT output.

The DUT waveforms are subsequently corrected for gain and time-base errors only if these errors are large relative to the reported uncertainties. The corrected or uncorrected waveforms are then used in a reconstruction process to obtain a waveform that is an accurate estimate of the pulse measured by the sampler. The accuracy of this estimate (the reconstructed waveform) is dependent on the reconstruction process and the accuracy of the estimate of the sampler impulse response. The waveform reconstruction process uses an iterative deconvolution of the sampler impulse response from the measured data. From each reconstructed waveform, pulse parameter values are computed. The set of pulse parameter values thus computed is used to determine the mean value and standard deviation for the given parameter.

The pulse parameter computations are based on histogram methods [11]. The first step in the calculations is to compute the histogram of the waveform. Next the top-line, V_{S2}, and bottom-line, V_{S1}, values are obtained from the histogram. Then, using V_{S2} and V_{S1}, the pulse parameters are obtained for the waveform.

This uncertainty analysis, because it is applied to acquired waveforms, is applicable to both the measurement of the output of pulse generators and the step response of samplers with the appropriate change in reference measurements and waveforms. When measuring the output of a pulse generator it is assumed that the sampler step response is the reference, and when measuring the sampler step response it is assumed that the output of the pulse generator is the reference.

3. Uncertainty analysis

The reported pulse parameters are an average of the particular pulse parameters obtained from a set of M_1 pulse waveforms measured using the NIST pulse measurement systems. The average of a parameter, W for example, is given by

$$\overline{W} = \frac{1}{M_1} \sum_{i=1}^{M_1} W_i(\alpha_j), \tag{1}$$

where M_1 is the number of values for the parameter W, one value for each waveform, and W is dependent on a number of variables, α_j. The uncertainty for this average, $\overline{W}$ for example, is given by

$$u_{\overline{W}} = k_{\text{eff}} \sqrt{\sum_{i=1}^{M_1} \left\{ \left(\frac{\partial \overline{W}}{\partial W_i} \right)^2 \left[\sum_j \left(\frac{\partial W_i(\alpha_j)}{\partial \alpha_j} \right)^2 u_j^2 \right] \right\}}$$

$$= k_{\text{eff}} \sqrt{\sum_{i=1}^{M_1} \left\{ \frac{1}{M_1^2} \sum_j \left[\left(\frac{\partial W_i(\alpha_j)}{\partial \alpha_j} \right)^2 u_j^2 \right] \right\}} \tag{2a}$$

$$= k_{\text{eff}} \sqrt{\frac{1}{M_1} \sum_j \left(\frac{\partial W_i(\alpha_j)}{\partial \alpha_j} \right)^2 u_j^2}, \tag{2b}$$

where it is assumed in (2a) that the α_j values are uncorrelated, which is the reason why there are no cross terms in the partial derivatives with respect to the α_j . In (2b) it is further assumed that the u_j values are the same for every W_i; that is, the uncertainties in the variables for a given parameter are the same for every waveform. The term k_{eff} is the statistical weight [12] applied to the uncertainties of variables obtained from a limited number of trials. For a number of variables with different degrees of freedom, k_{eff} is found by first calculating the effective degrees of freedom using [12]

$$\nu_{\text{eff}} = \frac{\left[\sum_{i=1}^{M} \left(\frac{\partial W(\alpha_1, \alpha_2, \ldots, \alpha_M)}{\partial \alpha_i} \right)^2 u_i^2 \right]^2}{\sum_{i=1}^{M} \frac{c_i^4 u_i^4}{\nu_i}}, \tag{3}$$

Table 1a. Variables affecting pulse amplitude uncertainty.

Variable α_i	Uncertainty[1] u_i	Partial derivative $\left\lvert \frac{\partial W(\alpha_1, \alpha_2, \ldots, \alpha_P)}{\partial \alpha_i} \right\rvert$	Type	Degrees of freedom ν_i
$V_{S2,m}$	$\sqrt{\sigma^2_{V_{S2,m}} + \left(\frac{\partial V_{S2,m}}{\partial H} u_H\right)^2}$	$\frac{1}{\sqrt{M_1}} \frac{1}{\overline{g}}$	A	$M_1 - 1$
$V_{S1,m}$	$\sqrt{\sigma^2_{V_{S1,m}} + \left(\frac{\partial V_{S1,m}}{\partial H} u_H\right)^2}$	$\frac{1}{\sqrt{M_1}} \frac{1}{\overline{g}}$	A	$M_1 - 1$
$\overline{g}$	$\sqrt{\sigma^2_{V_g} + \left(\frac{\partial g}{\partial V, H} u_{V,H}\right)^2}$	$\frac{\lvert V_A \rvert}{\overline{g}}$	A	$M_{10} - 1$
$\overline{T}_{meas}$	$\sigma_{T_{meas}}$	$\frac{S_{\Delta V/\Delta T}}{\overline{g}}$	A	$M_4 - 1$
$\overline{T}_{ref}$	$\sigma_{T_{ref}}$	$\frac{S_{\Delta V/\Delta T}}{\overline{g}}$	A	$M_5 - 1$
$S_{\Delta V/\Delta T}$	$\sigma_{S_{\Delta V/\Delta T}}$	$\frac{\overline{T}_{meas} - \overline{T}_{ref}}{\overline{g}}$	A	$M_6 - 2$

1. The letter V is used to represent amplitude-related uncertainty contributions to $\overline{g}$, see (8) and Table 1c. The letter H is used to represent histogram-related uncertainty contributions, see (11) and Table 1b.

Table 1b. Variables affecting the uncertainty in V_{S2} obtained using a histogram method.

Variable α_i	Uncertainty u_i	Partial derivative $\left\lvert \frac{\partial V_{S2}(\alpha_1, \alpha_2, \ldots, \alpha_P)}{\partial \alpha_i} \right\rvert$	Type	Degrees of freedom ν_i
V_{max}	$\sigma_{V_{max}}$ $(= 0)$	$\frac{N_{S2}}{N_{bins}}$	A	∞
V_{min}	$\sigma_{V_{min}}$ $(= 0)$	$\frac{N_{S2}}{N_{bins}}$	A	∞
N_{S2}	$u_{N_{S2}}$ $(= 0)$	$\frac{V_{max} - V_{min}}{N_{bins}}$	B	∞
N_{bins}	$u_{N_{bins}}$ $(\leq \pm 1/10 N_{bins})$	$\frac{V_{max} - V_{min}}{N^2_{bins}}$	B	∞

Table 1c. Variables affecting g.

Variable α_i	Uncertainty[1] u_i	Partial derivative $\left\lvert \frac{\partial W(\alpha_1, \alpha_2, \ldots, \alpha_P)}{\partial \alpha_i} \right\rvert$	Type	Degrees of freedom ν_i
$\overline{V}_{S2,m,r}$	$\sqrt{\sigma^2_{V_{S2,m,r}} + \left(\frac{\partial V_{S2,m,r}}{\partial H} u_H\right)^2}$	$\frac{1}{\sqrt{M_{10}}} \left\lvert \frac{1}{\overline{V}_{S2,r} - \overline{V}_{S1,r}} \right\rvert$	A	$M_2 - 1$
$\overline{V}_{S1,m,r}$	$\sqrt{\sigma^2_{V_{S1,m,r}} + \left(\frac{\partial V_{S1,m,r}}{\partial H} u_H\right)^2}$	$\frac{1}{\sqrt{M_{10}}} \left\lvert \frac{1}{\overline{V}_{S2,r} - \overline{V}_{S1,r}} \right\rvert$	A	$M_2 - 1$
$\overline{V}_{S2,r}$	$\sqrt{\sigma^2_{V_{S2,r}} + \left(\frac{\partial V_{S2,r}}{\partial H} u_H\right)^2}$	$\frac{1}{\sqrt{M_{10}}} \frac{\lvert \overline{V}_{S2,m,r} - \overline{V}_{S1,m,r} \rvert}{(\overline{V}_{S2,r} - \overline{V}_{S1,r})^2}$	A	$M_3 - 1$
$\overline{V}_{S1,r}$	$\sqrt{\sigma^2_{V_{S1,r}} + \left(\frac{\partial V_{S1,r}}{\partial H} u_H\right)^2}$	$\frac{1}{\sqrt{M_{10}}} \frac{\lvert \overline{V}_{S2,m,r} - \overline{V}_{S1,m,r} \rvert}{(\overline{V}_{S2,r} - \overline{V}_{S1,r})^2}$	A	$M_3 - 1$

1. The letter H is used to represent histogram-related uncertainty contributions see (11) and Table 1b.

Table 2a. Variables affecting pulse transition duration uncertainty.

Variable α_i	Uncertainty u_i	Partial derivative $\left\lvert\frac{\partial W(\alpha_1,\alpha_2,\ldots,\alpha_P)}{\partial\alpha_i}\right\rvert$	Type	Degrees of freedom ν_i
δt	$\sigma_{\delta t}$	$\frac{t_d}{\delta t}$	A	$M_{13}-1$
X_m	$\sqrt{\sigma^2_{X_m}+\left(\frac{\partial X_m}{\partial H}u_H\right)^2+\left(\frac{\partial X_m}{\partial T}u_T\right)^2}$ (see Tables 2b and 2d)	$\frac{1}{M_1}\sqrt{\sum_{i=1}^{M_1}\left(\frac{1}{\delta t}\left\lvert\frac{\partial t_{d.R.i}}{\partial t_{d.m.i}}\right\rvert\right)^2}$	A	M_1-1
X_r	$\sqrt{\sigma^2_{X_r}+\left(\frac{\partial X_r}{\partial H}u_H\right)^2}$ (see Table 2b)	$\frac{1}{M_1}\sqrt{\sum_{i=1}^{M_1}\left(\frac{1}{\delta t}\left\lvert\frac{\partial t_{d.R.i}}{\partial t_{d.r.i}}\right\rvert\right)^2}$	A	M_7-1
X_j	$\sqrt{\sigma^2_{X_j}+\left(\frac{\partial X_j}{\partial H}u_H\right)^2}$ (see Table 2b)	$\frac{1}{M_1}\sqrt{\sum_{i=1}^{M_1}\left(\frac{1}{\delta t}\left\lvert\frac{\partial t_{d.R.i}}{\partial t_{d.j}}\right\rvert\right)^2}$	A	$M_{12}-1$

Table 2b. Variables affecting X value uncertainty.

Variable α_i	Uncertainty u_i	Partial derivative $\left\lvert\frac{\partial W(\alpha_1,\alpha_2,\ldots,\alpha_P)}{\partial\alpha_i}\right\rvert$	Type	Degrees of freedom ν_i
m_{L1_-}	σ_{mL1_-} $(=0)$	$\frac{L1_+ - L1}{L1_+ - L1_-}$	A	∞
m_{L1_+}	σ_{mL1_+} $(=0)$	$\frac{L1 - L1_-}{L1_+ - L1_-}$	A	∞
m_{L2_-}	σ_{mL2_-} $(=0)$	$\frac{L2_+ - L2}{L2_+ - L2_-}$	A	∞
m_{L2_+}	σ_{mL2_+} $(=0)$	$\frac{L2 - L2_-}{L2_+ - L2_-}$	A	∞
$L1$	$\sqrt{\sigma^2_{L1}+\left(\frac{\partial L1}{\partial\alpha_i}u_{\alpha_i}\right)^2}$ (see Table 2c)	$(m_{L1_+}-m_{L1_-})\frac{1}{L1_+ - L1_-}$	A	∞
$L1_-$	σ_{L1_-} $(=0)$	$(m_{L1_+}-m_{L1_-})\frac{L1_+ - L1}{(L1_+ - L1_-)^2}$	A	∞
$L1_+$	σ_{L1_+} $(=0)$	$(m_{L1_+}-m_{L1_-})\frac{L1 - L1_-}{(L1_+ - L1_-)^2}$	A	∞
$L2$	$\sqrt{\sigma^2_{L2}+\left(\frac{\partial L2}{\partial\alpha_i}u_{\alpha_i}\right)^2}$ (see Table 2)	$(m_{L2_+}-m_{L2_-})\frac{1}{L2_+ - L2_-}$	A	∞
$L2_-$	σ_{L2_-} $(=0)$	$(m_{L2_+}-m_{L2_-})\frac{L2_+ - L2}{(L2_+ - L2_-)^2}$	A	∞
$L2_+$	σ_{L2_+} $(=0)$	$(m_{L2_+}-m_{L2_-})\frac{L2 - L2_-}{(L2_+ - L2_-)^2}$	A	∞

where ν_i is the number of degrees of freedom for the parameters (shown in Tables 1 to 4) and c_i are the partial differential equations (shown in Tables 1 to 4). Weight k_{eff} is then found from ν_{eff} using the t-distribution [12].

The uncertainties in the variables, u_i (where the subscript refers to parameter i), are obtained from independent measurements that provide values for these particular variables. The tables list the source of u_i for the appropriate variables. To calculate the uncertainty of the different parameters, the partial derivatives of these parameters with respect to the independent variables must be calculated. These partial derivatives are also

Table 2c. Variables affecting uncertainty of L_1 and L_2.

Variable α_i	Uncertainty u_i	Partial derivative $\left\lvert \frac{\partial W(\alpha_1, \alpha_2, \ldots \alpha_P)}{\partial \alpha_i} \right\rvert$	Type	Degrees of freedom ν_i
$V_{S1,m}$	see Table 1a	$1 - P\%$	A	∞
$V_{S2,m}$	see Table 1a	$P\%$	A	∞

Table 2d. Variables affecting uncertainty of X_m.

Variable α_i	Uncertainty u_i	Partial derivative $\left\lvert \frac{\partial W(\alpha_1, \alpha_2, \ldots \alpha_P)}{\partial \alpha_i} \right\rvert$	Type	Degrees of freedom ν_i
$S_{\Delta t/\Delta T}$	$\sigma_{S_{\Delta t/\Delta T}}$	$\overline{T}_{meas} - \overline{T}_{ref}$	A	$M_8 - 2$
$\overline{T}_{meas}$	$\sigma_{T_{meas}}$	$S_{\Delta t/\Delta T}$	A	$M_4 - 1$
$\overline{T}_{ref}$	$\sigma_{T_{ref}}$	$S_{\Delta t/\Delta T}$	A	$M_5 - 1$

Table 3. Variables affecting uncertainty in pulse overshoot.

Variable α_i	Uncertainty[1] u_i	Partial derivative $\left\lvert \frac{\partial W(\alpha_1, \alpha_2, \ldots \alpha_P)}{\partial \alpha_i} \right\rvert$	Type	Degrees of freedom ν_i
$V_{max,m}$	$\sigma_{V_{max,m}}$ $(= 0)$	$\frac{1}{M_1}\sqrt{\sum_{i=1}^{M_1}\left(\beta_O \frac{X_{m,i}}{X_{R,i}} \frac{1}{V_{A,R,i}}\right)^2}$	A	∞
$V_{S2,m}$	$\sigma'_{V_{S2,m}}$	$\frac{1}{M_1}\sqrt{\sum_{i=1}^{M_1}\left(\beta_O \frac{X_{m,i}}{X_{R,i}} \frac{1}{V_{A,R,i}}\right)^2}$	A	∞
$V_{S2,R}$	$\sigma'_{V_{S2,R}}$	$\frac{1}{M_1}\sqrt{\sum_{i=1}^{M_1}\left[\left(\frac{1}{V^2_{A,R,i}}\right)\left(\beta_O[V_{max,m,i} - V_{S2,m,i}]\frac{X_{m,i}}{X_{R,i}}\right)\right]^2}$	A	∞
$V_{S1,R}$	$\sigma'_{V_{S1,R}}$	$\frac{1}{M_1}\sqrt{\sum_{i=1}^{M_1}\left[\left(\frac{1}{V^2_{A,R,i}}\right)\left(\beta_O[V_{max,m,i} - V_{S2,m,i}]\frac{X_{m,i}}{X_{R,i}}\right)\right]^2}$	A	∞
X_m	$\sqrt{\sigma^2_{X_m} + \left(\frac{\partial X_m}{\partial H} u_H\right)^2}$ (see Tables 2b and 2c)	$\frac{1}{M_1}\sqrt{\sum_{i=1}^{M_1}\left(\beta_O[V_{max,m,i} - V_{S2,m,i}]\frac{X_{m,i}}{X_{R,i}} \frac{1}{V_{A,R,i}}\right)^2}$	A	∞
X_d	$\sqrt{\sigma^2_{X_R} + \left(\frac{\partial X_R}{\partial H} u_H\right)^2}$ (see Tables 2b and 2c)	$\frac{1}{M_1}\sqrt{\sum_{i=1}^{M_1}\left(\beta_O[V_{max,m,i} - V_{S2,m,i}]\frac{X_{m,i}}{X^2_{R,i}} \frac{1}{V_{A,R,i}}\right)^2}$	A	∞
β_O	σ_{β_O}	$\frac{1}{M_1}\sqrt{\sum_{i=1}^{M_1}\left([V_{max,m,i} - V_{S2,m,i}]\frac{X_{m,i}}{X_{R,i}} \frac{1}{V_{A,R,i}}\right)^2}$	A	$M_9 - 2$

1. The prime notation indicates that the uncertainty for these parameters must include histogram-dependent uncertainties, as for the example V_{S2} in Section 3.1. That is, the prime notation indicates

$$\sigma' = \sqrt{\sigma^2 + \left(\frac{\partial V}{\partial H} u_H\right)^2}. \tag{33}$$

Table 4. Variables affecting uncertainty in pulse undershoot.

Variable α_i	Uncertainty[1] u_i	Partial derivative $\left\lvert \frac{\partial W(\alpha_1, \alpha_2, \ldots, \alpha_P)}{\partial \alpha_i} \right\rvert$	Type	Degrees of freedom ν_i
$V_{\min,m}$	$\sigma_{V_{\min,m}}$ $(= 0)$	$\frac{1}{M_1}\sqrt{\sum_{i=1}^{M_1}\left(\beta_{t'}\cdot\frac{X_{m,i}}{X_{R,i}}\frac{1}{V_{A,R,i}}\right)^2}$	A	∞
$V_{S1,m}$	$\sigma'_{V_{S1,m}}$	$\frac{1}{M_1}\sqrt{\sum_{i=1}^{M_1}\left(\beta_{t'}\cdot\frac{X_{m,i}}{X_{R,i}}\frac{1}{V_{A,R,i}}\right)^2}$	A	∞
$V_{S2,R}$	$\sigma'_{V_{S2,R}}$	$\frac{1}{M_1}\sqrt{\sum_{i=1}^{M_1}\left[\left(\frac{1}{V^2_{A,R,i}}\right)\left(\beta_{t'}\cdot[V_{\min,m,i}-V_{S1,m,i}]\frac{X_{m,i}}{X_{R,i}}\right)\right]^2}$	A	∞
$V_{S1,R}$	$\sigma'_{V_{S1,r}}$	$\frac{1}{M_1}\sqrt{\sum_{i=1}^{M_1}\left[\left(\frac{1}{V^2_{A,R,i}}\right)\left(\beta_{t'}\cdot[V_{\min,m,i}-V_{S1,m,i}]\frac{X_{m,i}}{X_{R,i}}\right)\right]^2}$	A	∞
X_m	$\sqrt{\sigma^2_{X_m}+\left(\frac{\partial X_m}{\partial H}u_H\right)^2}$ (see Tables 2b and 2c)	$\frac{1}{M_1}\sqrt{\sum_{i=1}^{M_1}\left(\beta_{t'}\cdot[V_{\min,m,i}-V_{S1,m,i}]\frac{1}{X_{R,i}}\frac{1}{V_{A,R,i}}\right)^2}$	A	∞
X_d	$\sqrt{\sigma^2_{X_R}+\left(\frac{\partial X_R}{\partial H}u_H\right)^2}$ (see Tables 2b and 2c)	$\frac{1}{M_1}\sqrt{\sum_{i=1}^{M_1}\left(\beta_{t'}\cdot[V_{\min,m,i}-V_{S1,m,i}]\frac{X_{m,i}}{X^2_{R,i}}\frac{1}{V_{A,R,i}}\right)^2}$	A	∞
$\beta_{t'}$	$\sigma_{\beta_{t'}}$	$\frac{1}{M_1}\sqrt{\sum_{i=1}^{M_1}\left([V_{\min,m,i}-V_{S1,m,i}]\frac{X_{m,i}}{X_{R,i}}\frac{1}{V_{A,R,i}}\right)^2}$	A	$M_{11}-2$

1. The prime notation indicates that the uncertainty for these parameters must include histogram-dependent uncertainties, as for the example V_{S2} in Section 3.1 (see also (33)).

shown in the tables. The tables for each variable include its type of uncertainty [12] and degrees of freedom, ν. For measured data, the number of degrees of freedom is given by $\nu = M_k - 1$, where M_k is the number of data elements used to compute the value of the k-th variable. For fits to data, ν is given by $\nu = M_k - m_k$, where m_k is the number of coefficients used to fit the data. The number of degrees of freedom for certain variables is equal to infinity ($\nu = \infty$) because the calculation of the value of these variables is based on a specific fixed waveform. Accordingly, every (an infinite set) computation of the value of that variable for that waveform yields the same result.

The variation in measurements, represented by the symbol σ in the tables and text, is unless otherwise indicated the standard deviation of a set of measurement values of a given parameter or the standard deviation of the residuals of a curve fitted to the data. For example, of the first case, $\sigma_{V_{S2,m}}$ in Table 1a is the standard deviation of M_1 values, one $V_{S2,m}$ value taken from each of the M_1 measured (acquired) waveforms. For example, of the second case, the $\sigma_{S_{\Delta V/\Delta T}}$ in Table 1a is the standard deviation of the residuals to a fit to the amplitude versus temperature data.

3.1 Pulse amplitude

The pulse amplitude is obtained using a histogram-based algorithm (see Section 2). The pulse amplitude is the difference between V_{S2} and V_{S1}. Calculating the uncertainty in the pulse amplitude requires an equation that describes the reported pulse amplitude, V_A:

$$V_A = \frac{\overline{V_{A,c/r}}}{\overline{g}}, \tag{4}$$

where the horizontal bars indicate the arithmetic mean, $\overline{V}_{A,c/r}$ is the mean of the set of M_1 pulse amplitudes corrected for sampler offset errors and waveform reconstruction errors, and $\overline{g}$ is the mean of the transient amplitude gain correction of the sampler. A common practice in oscilloscope calibrations is to use or include a static level gain-correction term in (4). However, since the signals being measured are transients (steps or impulses), as opposed to static levels, a transient gain term, the $\overline{g}$ in (4), should be used. The transient gain is affected by the impulse response of the sampler and the waveform epoch because of the settling response of the sampler. For example, if the sampler response has not settled by the end of the epoch, then g will be less than one for that epoch. Ideally, $\overline{g} = 1$ if the sampler exhibits no pulse gain or attenuation and the sampler has settled within the waveform epoch. The $\overline{V}_{\mathrm{A,c/r}}$ is given by

$$\begin{aligned}\overline{V}_{\mathrm{A,c/r}} &= \overline{V}_{\mathrm{A,c}}b_{\mathrm{r}} = (\overline{V}_{\mathrm{S2,c}} - \overline{V}_{\mathrm{S1,c}})b_{\mathrm{r}} \\ &= [\overline{V}_{\mathrm{S2,m}} - \overline{V}_{\mathrm{S2,off,m}} - (\overline{V}_{\mathrm{S1,m}} - \overline{V}_{\mathrm{S1,off,m}}) + \\ &\quad \overline{V}_{\Delta T}]b_{\mathrm{r}},\end{aligned} \tag{5}$$

where $\overline{V}_{\mathrm{off}}$ is the voltage offset, which is a bias in the observed voltage, $\overline{V}_{\mathrm{A,c}}$ is the mean of the set of M_1 pulse amplitudes corrected for sampler offset errors, $\overline{V}_{\Delta T}$ is the mean of the amplitude corrections required for a change in measurement temperature, and β_{r} reflects the error in the amplitude of the reconstructed waveform caused by the reconstruction process. Ideally, β_{r} should be 1 because the sampler impulse response estimates integrate to 1. However, the reconstruction process introduces an error in the amplitude. This scaling error is exactly corrected by rescaling the pulse amplitude of the reconstructed waveform to equal $\overline{V}_{\mathrm{A,c}}$. The subscripts c and m refer to corrected and measured voltage values. We have observed that for the currently available high-bandwidth samplers, the voltage offset error is the same for both the top-line (S2) and bottom-line (S1) voltage levels; therefore, the offset voltage contribution can be ignored.

The temperature-correction term is obtained by measuring the change in the observed pulse amplitude with temperature [13]. The $\overline{V}_{\Delta T}$ term is therefore

$$\overline{V}_{\Delta T} = S_{\Delta V/\Delta T}(\overline{T}_{\mathrm{meas}} - \overline{T}_{\mathrm{ref}}), \tag{6}$$

where $\overline{T}_{\mathrm{meas}}$ is the average of M_4 sampler temperature values taken during the pulse measurement process, S is the slope of a straight-line fit through a set of previously acquired amplitude versus temperature data, and $\overline{T}_{\mathrm{ref}}$ is the average reference sampler temperature that is taken to be the mean of M_5 temperature values of the sampling head measured when the sampler impulse response was determined. The amplitude versus temperature data consist of a set of M_6 data pairs and are recorded over a temperature range between T_2 and T_1; the difference between these two temperatures is ΔT. Every sampler may exhibit a unique temperature-dependent response.

Amplitude V_{A} can now be rewritten using (5) and (6) in (4):

$$V_{\mathrm{A}} = \frac{(\overline{V}_{\mathrm{S2,m}} - \overline{V}_{\mathrm{S1,m}})}{\overline{g}} + \frac{S_{\Delta V/\Delta T}(\overline{T}_{\mathrm{meas}} - \overline{T}_{\mathrm{ref}})}{\overline{g}}. \tag{7}$$

The transient gain term, $\overline{g}$, is obtained by taking the ratio of the amplitude of the reference pulse as measured using the sampler and the amplitude of the reference pulse as measured using a reference instrument [14], which provides more accurate pulse amplitude measurements than high-speed samplers. As mentioned above, the gain term is obtained from a control chart and is given by

$$\begin{aligned}\overline{g} &= \frac{1}{M_{10}}\sum_{i=1}^{M_{10}} g_i \\ &= \frac{1}{M_{10}}\sum_{i=1}^{M_{10}} \frac{\overline{V}_{\mathrm{S2,m,r,i}} - \overline{V}_{\mathrm{S1,m,r,i}}}{\overline{V}_{\mathrm{S2,r,i}} - \overline{V}_{\mathrm{S1,r,i}}},\end{aligned} \tag{8}$$

where the subscript r denotes the reference pulse measurement and there are M_{10} independent gain terms. Using the ratio of average amplitudes in (8) is numerically more stable than an average of the amplitude ratios. Furthermore, the ratio of the average amplitudes relaxes the requirement that a reference measurement be made for each sampler-acquired measurement. A set of M_2 measurements of the reference pulse are used to obtain the reference-instrument-measured parameters and a set of M_3 measurements of the reference pulse are used to obtain the sampler-measured parameters. Temperature-dependent gain effects are included in $V_{\Delta T}$, which describes the change in pulse amplitude with change in temperature relative to T_{ref}. The g_i were computed from data taken at T_{ref}.

The variables shown in (8) contribute to the uncertainty in V_{A}. The uncertainty in V_{A}, $u_{V_{\mathrm{A}}}$, is dependent on the uncertainties of all the variables from which V_{A} is dependent, and these variables are listed in Tables 1a and 1b. The uncertainties, u_i, in the variables are obtained from independent measurements that provide values for these particular variables. Table 1a lists the source of u_i for the appropriate variables. The partial derivatives of V_{A} with respect to the independent variables are also shown in Table 1a, as are its associated degrees of freedom and uncertainty type [11]. $\overline{T}_{\mathrm{meas}}$, although obtained from M_1 averages of the average of M_4 temperature measurements taken during each waveform acquisition, has $\nu = M_1 - 1$. The uncertainties for $S_{\Delta V/\Delta T}$ require an empirical formula relating the pulse amplitude of the acquired waveform to temperature (see Figure 2) which is obtained by fitting a curve, typically a line, to the data.

In addition to measurement-related uncertainties, the reported amplitude values are also subject to uncertainties from the method used to calculate these values, in this case a histogram. The histogram-derived amplitude values, for example for V_{S2}, are given by

$$V_{\mathrm{S2}} = N_{\mathrm{S2}}\Delta V + V_{\mathrm{min}}, \tag{9}$$

where

$$\Delta V = \frac{V_{\mathrm{max}} - V_{\mathrm{min}}}{N_{\mathrm{bins}}}, \tag{10}$$

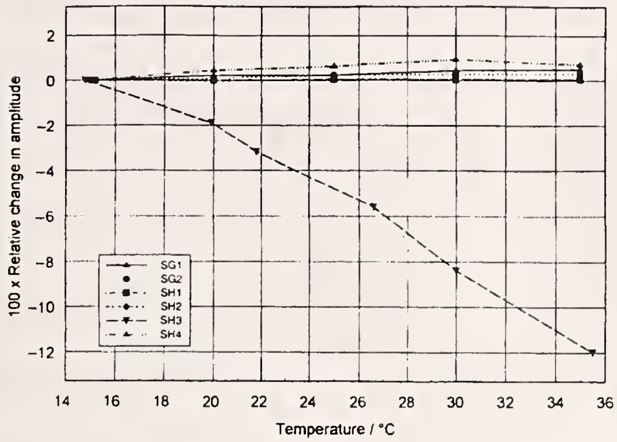

Figure 2. The percentage change in pulse amplitude with temperature relative to 15 °C. The designation SG refers to step generator and SH to sampling head. The number following the designation refers to models of devices made by different manufacturers.

and ΔV is the histogram bin size and N_{bins} is the number of histogram bins. The uncertainty contribution associated with V_{S2}, for example, is then

$$\frac{\partial V_{\mathrm{S2}}}{\partial H} u_H = \frac{1}{N_{\mathrm{bins}}} \times \sqrt{ (V_{\max} - V_{\min})^2 u_{N_{\mathrm{S2}}}^2 + N_{\mathrm{S2}}^2 \times \left[\sigma_{V_{\max}}^2 + \sigma_{V_{\min}}^2 + \frac{1}{N_{\mathrm{bins}}^2} (V_{\max} - V_{\min})^2 u_{N_{\mathrm{bins}}}^2 \right] }. \quad (11)$$

The term H is used as a place holder to represent all the histogram-based dependences of a variable, such as V_{S2} in the example of (11). Table 1b, used as an example, lists variables affecting the V_{S2} amplitude variables. All amplitude values listed in the first column of Table 1a have an analogous list of variables. The degrees of freedom are infinite for N_{S2} and N_{bins} because they are extracted using a given pulse parameter algorithm and the output of this algorithm will not vary for a given waveform. The degrees of freedom are infinite for $V_{\max}$ and $V_{\min}$ because these values, for a given waveform, are fixed once a waveform has been acquired.

3.2 Transition duration

The transition duration is the difference between the occurrences of user-defined amplitude reference levels, for example, the 10 % and 90 % amplitude reference levels. The times at which the waveform crosses these reference levels are called reference-level instants. Accordingly, the 10 % to 90 % transition duration is the difference between the 90 % and 10 % reference level instants.

The reported waveform transition duration, t_{d}, is the average transition duration extracted from M_1 reconstructed pulse waveforms, $t_{\mathrm{d,R}}$. Duration t_{d} is related to the transition duration of the acquired waveform, $t_{\mathrm{d,m}}$, and the transition duration of the estimated sampler step response, $t_{\mathrm{d,r}}$:

$$t_{\mathrm{d}} = \frac{1}{M_1} \sum_{i=1}^{M_1} t_{\mathrm{d,R,}i} \times \overline{f_{\mathrm{dec}}(t_{\mathrm{d,m}} + \Delta t_{\mathrm{d,}\Delta T} t_{\mathrm{d,r}}) + \Delta t_{\mathrm{d,rec}}}. \quad (12)$$

where $\Delta t_{\mathrm{d,}\Delta T}$ is the temperature-induced incremental change in transition duration [13] (described below), $\Delta t_{\mathrm{d,rec}}$ is the bias in the transition duration caused by the reconstruction process, and f_{dec} is used to indicate the deconvolution functional relationship between $t_{\mathrm{d,R}}$, $t_{\mathrm{d,m}}$ and $t_{\mathrm{d,r}}$. Duration $t_{\mathrm{d,R}}$ is found from a waveform that is obtained by deconvolving a waveform with transition duration $t_{\mathrm{d,r}}$ from a waveform with transition duration $t_{\mathrm{d,m}}$. The specific functional relationship, f_{dec}, between t_{d}, $t_{\mathrm{d,m}}$, and $t_{\mathrm{d,r}}$ is dependent on the type of waveform used and can only be derived for certain ideal waveforms. For example, for Gaussian waveforms, t_{d} is equal to the square root of the difference of the squares of transition durations of the measured and step response waveforms. For general waveforms, we can obtain an empirical relationship relating the three parameters. The first step in obtaining this empirical relationship is to vary either $t_{\mathrm{d,m}}$ or $t_{\mathrm{d,r}}$ in the waveform reconstruction process, keeping the other constant, and noting the variation in $t_{\mathrm{d,R}}$. This provides two sets of data, one relating $t_{\mathrm{d,R}}$ to $t_{\mathrm{d,m}}$ for a fixed $t_{\mathrm{d,r}}$ and another relating $t_{\mathrm{d,R}}$ to $t_{\mathrm{d,r}}$ for a fixed $t_{\mathrm{d,m}}$. We obtain our empirical relationship by fitting a curve (such as a polynomial) to these sets of data, $t_{\mathrm{d,m}}$ versus $t_{\mathrm{d,R}}$ and $t_{\mathrm{d,r}}$ versus $t_{\mathrm{d,R}}$. The reconstruction process we now use is described in [15]. However, we are also investigating various filtering methods, one of which is discussed in [16]. Using our present reconstruction algorithms on known waveforms, we have observed a bias, $\Delta t_{\mathrm{d,rec}}$, and a noise-dependent variation in $t_{\mathrm{d,R}}$. The noise-dependent variation is also contained in the empirical relationship, but the bias is not. Therefore, the uncertainty for the reconstruction process is computed by adding the absolute value of the bias to the computed uncertainty.

The parameters $t_{\mathrm{d,m}}$ and $t_{\mathrm{d,r}}$ can be expressed in terms of the sampling intervals:

$$t_{\mathrm{d,m}} = X_{\mathrm{m}} \delta t, \qquad t_{\mathrm{d,r}} = X_{\mathrm{rj}} \delta t, \quad (13)$$

where X_{m} and X_{rj} are the real-valued (non-integer) number of sampling intervals describing the transition duration for the measured sampler step response waveforms (including jitter) and δt is the duration of the equispaced sampling interval. X_{rj} is computed from waveforms that are the result of the convolution of the

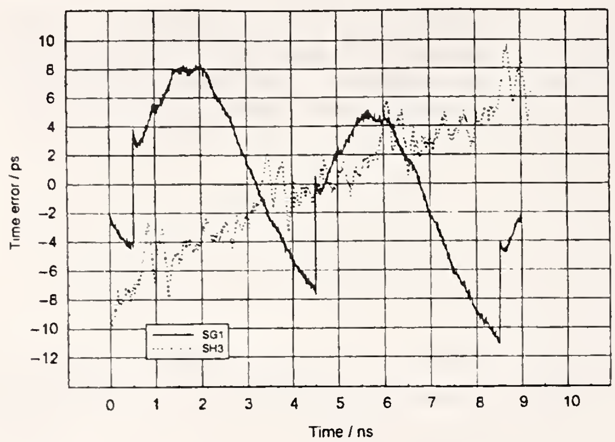

Figure 3. Time-base errors. The designation SG refers to step generator and SH to sampling head. The number following the designation refers to different models of devices made by different manufacturers.

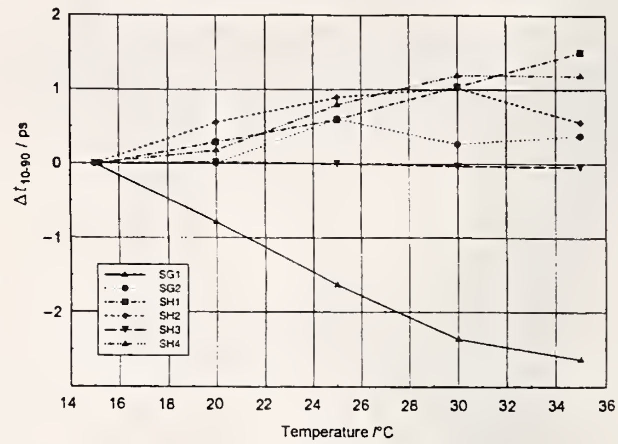

Figure 4. The change in transition duration, $\Delta t_{10\text{-}90}$, with temperature relative to 15 °C. The designation SG refers to step generator and SH to sampling head. The number following the designation refers to models of devices made by different manufacturers.

system jitter, represented by a Gaussian waveform, and the sampler step response, obtained from the sampler calibration method. The result of this convolution, estimated using the Gaussian approximation, is

$$X_{\mathrm{rj}} \approx \sqrt{X_{\mathrm{r}}^2 + X_{\mathrm{j}}^2}, \tag{14}$$

where X_{r} and X_{j} are the number of sampling intervals in the sampler step response and equivalent jitter step response transition durations. However, there are errors associated with this approximation [17]. For this uncertainty analysis the convolutions of the two waveforms are performed numerically and the resultant waveform used in subsequent processing. The measurement jitter typically has a normal distribution. We approximate X_{j} using a direct measurement taken by the sampler. We have observed that estimates of the jitter obtained employing a geometric method [18] are very sensitive to the transition region from which the estimate is made. Term X_{j} includes drift of the sampling aperture with respect to its trigger. Term δt is the average duration of the sampling intervals that span either the transition region of the waveform or the entire waveform [19] and is measured using sine-fit techniques [9] during the time-base calibration process. Figure 3 shows an example of time-base errors (vertical axis) versus measurement time. One time-base calibration is performed for each waveform; therefore the variation in δt is the variation of δt among the M_1 acquired waveforms. Similarly, the variation in X_{m} is dependent on the set of M_1 acquired waveforms. The variation in X_{r} is dependent on the set of M_7 acquired reference waveforms. The variation in X_{j} is dependent on the set of M_{12} jitter measurements. The temperature-dependent change in transition duration can be expanded:

$$\Delta t_{\mathrm{d},\Delta T} = S_{\Delta t/\Delta T}(\overline{T}_{\mathrm{meas}} - \overline{T}_{\mathrm{ref}}), \tag{15}$$

where $S_{\Delta t/\Delta T}$ is the slope of a straight-line fit to M_8 transition-duration-temperature data pairs (see Figure 4), measured independently of the M_1 acquired waveforms. Using (13) and (15) in (12) gives

$$t_{\mathrm{d}} = \overline{f_{\mathrm{dec}}[X_{\mathrm{m}}\delta t + S_{\Delta t/\Delta T}(\overline{T}_{\mathrm{meas}} - \overline{T}_{\mathrm{ref}})X_{\mathrm{rj}}\delta t]} + \Delta t_{\mathrm{d,rec}}. \tag{16}$$

For the samplers and pulse generators currently in use at the NIST, the value of $\Delta t_{\mathrm{d},\Delta T}$ is approximated as zero because it is much less than the reported uncertainties; however, it is retained here for completeness. As we did in the pulse amplitude uncertainty analysis, we generate a table for the variables contributing to the transition duration value (see Table 2a).

The values of X_{m}, X_{r} and X_{j} are determined by linearly interpolating to obtain the instant in time (the reference-level instant) corresponding to the given reference level. The value of X_{m} (and analogously for X_{r} and X_{j}), is

$$X_{\mathrm{m}} = \frac{t_{L_2} - t_{L_1}}{\delta t}, \tag{17}$$

where t_{L_1} and t_{L_2} are the time instances corresponding to the first (L_1) and second (L_2) reference levels of the transition duration. For example, in the 10 % to 90 % transition duration, L_1 is the 10 % reference-level instant and L_2 is the 90 % reference-level instant. Instant t_{L_1} is given by

$$t_{L_1} = t_{L_{1-}} + \frac{t_{L_{1+}} - t_{L_{1-}}}{L_{1+} - L_{1-}}(L_1 - L_{1-}), \tag{18}$$

where the subscripts + and − denote the actual sampling instances found on either side of the reference-level instant (either t_{L_1} or t_{L_2}) and the data values corresponding to the reference-level instants. Similarly, t_{L_2} is given by

$$t_{L_2} = t_{L_{2-}} + \frac{t_{L_{2+}} - t_{L_{2-}}}{L_{2+} - L_{2-}}(L_2 - L_{2-}). \quad (19)$$

Using (18) and (19) in (17) yields

$$X_m = \left[t_{L_{2-}} + \frac{t_{L_{2+}} - t_{L_{2-}}}{L_{2+} - L_{2-}}(L_2 - L_{2-}) - t_{L_{1-}} - \frac{t_{L_{1+}} - t_{L_{1-}}}{L_{1+} - L_{1-}}(L_1 - L_{1-})\right]/\delta t$$
$$= m_{L_{2-}} - m_{L_{1-}} + (m_{L_{2+}} - m_{L_{2-}}) \times \frac{L_2 - L_{2-}}{L_{2+} - L_{2-}} - (m_{L_{1+}} - m_{L_{1-}})\frac{L_1 - L_{1-}}{L_{1+} - L_{1-}}, \quad (20)$$

where the m_L terms are the time indices corresponding to the actual data found immediately above and below the reference levels. Using (20), we can obtain the uncertainty expansion for X_m (and, similarly, for X_r and X_j), which is shown in Table 2b. All the variables listed in Table 2b are extracted using our pulse parameter algorithm and, consequently, the degrees of freedom are infinite. The values of L_1 and L_2 can be expanded:

$$L_1 = \overline{V}_{S1,m} + P_1(V_{S2,m} - V_{S1,m}),$$
$$L_2 = \overline{V}_{S1,m} + P_2(V_{S2,m} - V_{S1,m}), \quad (21)$$

where P_1 and P_2 are the percentage reference values, such as 10 % and 90 % or 20 % and 80 %. Table 2c provides an uncertainty assessment for L_1 and L_2.

3.3 Overshoot

Overshoot is, for waveforms with positive-going transitions, the maximum positive amplitude excursion relative to V_{S2} that the waveform makes near the transition region. On the other hand, for waveforms with negative-going transitions, overshoot is the maximum negative amplitude excursion relative to V_{S2} that the waveform makes near the transition region. For overshoot, we currently define "near the transition region" to be that period between the 50 % reference-level instant ($t_{50\%}$) and $t_{50\%} + 3t_d$ (IEEE TC-10 Subcommittee on Pulse Techniques). Voltage offset errors are not considered here because they cancel, as they did for the uncertainty calculation of $V_{A,c}$. The equation describing the calculation for the overshoot is

$$O = \overline{\left(\frac{V_{max,R} - V_{S2,R}}{V_{A,R}}\right)} + \Delta O_{rec}, \quad (22)$$

where ΔO_{rec} is the reconstruction-induced bias in the overshoot of the reconstructed waveform. $V_{max,R}$ may be written

$$V_{max,R} = V_{S2,R} + V_{O,R}, \quad (23)$$

where

$$V_{O,R} = \frac{\beta_O V_{O,m} t_{d,m}}{t_{d,R}}, \quad (24)$$

and β_O is a correction factor that is needed because of the reconstruction process and is found by fitting a curve to an M_9-element set of $t_{d,m}V_{O,m}$ versus $t_{d,R}V_{O,R}$ data. The $t_{d,m}$ and $V_{O,m}$ parameters are obtained from the acquired waveforms and $t_{d,R}$ and $V_{O,R}$ from the reconstructed waveforms. Equation (24) describes an empirical relationship between the overshoot and transition duration of the reconstructed (reported) waveform and those of the acquired waveform. As with transition duration (see Section 3.2), we have observed a bias and a noise-dependent variation in $V_{O,R}$ caused by the waveform reconstruction: the noise-dependent variation is contained in the empirical relationship but the bias is not. Therefore, the uncertainty in overshoot is computed by adding the computed uncertainty to the absolute value of the bias. In (24), we assume that the product of the overshoot voltage and transition duration is not affected by an all-pass filter, which is how the sampler impulse response is expected to behave for an input signal that has a 3 dB attenuation bandwidth lower than that of the sampler. The uncertainties in $t_{d,r}$ are included in the uncertainty estimate of $V_{O,R}$ by propagation of uncertainties through $t_{d,R}$. $V_{O,m}$ can be expanded:

$$V_{O,m} = V_{max,m} - V_{S2,m}. \quad (25)$$

Parameter $t_{d,R}$ can be expanded in a similar way to $t_{d,m}$ (13):

$$t_{d,R} = X_R \delta t, \quad (26)$$

where X_d is the non-integer number of sampling intervals describing the transition duration of the reconstructed waveform. Using (13), (23), (24), (25) and (26) in (22) yields for O:

$$O = \overline{\left(\frac{1}{V_{S2,R} - V_{S1,R}}\right)\left(\beta_O[V_{max,m} - V_{S2,m}]\frac{X_m}{X_R}\right)} + \Delta O_{rec}. \quad (27)$$

The uncertainty in β_O is the standard deviation in the fitted curve relative to the set of corresponding $t_{d,m}V_{O,m}$ versus $t_{d,R}V_{O,R}$ data and the coverage factor is determined by the number of β_O values. Table 3 shows the uncertainty-related parameters for the variables affecting O.

3.4 Undershoot (preshoot)

Undershoot is, for waveforms with positive-going transitions, the maximum negative amplitude excursion relative to V_{S1} that the waveform makes near the transition region. On the other hand, for waveforms with negative-going transitions, undershoot is the maximum positive amplitude excursion relative to V_{S1} that the waveform makes near the transition region. For undershoot, we currently define "near the transition region" to be that period between the $t_{50\%} - 3t_d$ and $t_{50\%}$ (IEEE TC-10 Subcommittee on Pulse Techniques). Voltage offset errors are not considered here because they cancel, as they did for the uncertainty calculation of $V_{A,c}$. The equation describing the calculation for the undershoot is

$$U = \overline{\left(\frac{V_{\min,R} - V_{S1,R}}{V_{A,R}}\right)} + \Delta U_{rec}, \tag{28}$$

where ΔU_{rec} is the reconstruction-induced bias in the undershoot of the reconstructed waveform. $V_{\min,R}$ may be written

$$V_{\min,R} = V_{S1,R} + V_{U,R}, \tag{29}$$

where

$$V_{U,R} = \frac{\beta_U V_{U,m} t_{d,m}}{t_{d,R}}, \tag{30}$$

and β_U is a correction factor that is determined experimentally as for β_O. Equation (30) provides an empirical relationship between the undershoot and transition duration of the reconstructed (reported) waveform and that of the acquired waveform. As with overshoot (see Section 3.3), we have observed a bias and a noise-dependent variation in $V_{U,R}$ caused by the waveform reconstruction. The uncertainty in undershoot is computed by adding the computed uncertainty to the absolute value of the bias. We assume that the product of the undershoot voltage and transition duration is not affected by an all-pass filter, which is how the sampler impulse response is expected to behave for an input signal that has a 3 dB attenuation bandwidth lower than that of the sampler. $V_{U,m}$ can be expanded:

$$V_{U,m} = V_{\min,m} - V_{S1,m}. \tag{31}$$

Using (13), (26), (29), (30), and (31) in (28) yields for U:

$$U = \overline{\left(\frac{1}{V_{S2,R} - V_{S1,R}}\right)\left(\beta_U [V_{\min,m} - V_{S1,m}] \frac{X_m}{X_R}\right)} + \Delta U_{rec}. \tag{32}$$

The correction factor β_U is determined by fitting a curve to an M_9-element set of $t_{d,m} V_{U,m}$ versus $t_{d,R} V_{U,R}$ data. The uncertainty in β_U is the standard deviation in the fitted curve relative to the set of corresponding $t_{d,m} V_{U,m}$ versus $t_{d,R} V_{U,R}$ data and the coverage factor is determined by the number of β_U values. Table 4 shows the uncertainty-related parameters for the variables affecting U.

4. Summary

A detailed uncertainty analysis of the parameters transition duration, overshoot, undershoot and amplitude of step-like waveforms was performed. This analysis included a consideration of effects that can affect the value of the reported parameters, such as temperature, computation algorithms, history of instrument performance, equipment limitations and estimates of the response characteristics of the instrument. Our present published uncertainties, which are the result of the new measurement process and associated uncertainty analysis, for high-speed (7 ps < t_d < 350 ps) pulse generators and samplers are ±2 mV for pulse amplitude and ±1.5 ps for transition duration. Our measured uncertainties, however, are smaller.

Acknowledgements. We would like to thank W. F. Guthrie and G. N. Stenbakken of the NIST, Gaithersburg, Md., and D. C. DeGroot of the NIST, Boulder, Colo., for technical comments and B. A. Bell of the NIST, Gaithersburg, for administrative support.

References

1. *NIST Calibration Services Users Guide,* NIST Spec. Publ. SP250, Washington, D.C., U.S. Dept. of Commerce, 1998, 189-193.
2. Paulter N. G., Larson D. R., *Improving the uncertainty analysis of NIST's pulse parameter measurement service*, Automatic Radio Frequency Techniques Group, 56th Conference, Boulder, Colo., 30 November to 1 December 2000.
3. Rush K., Draving S., Kerley J., *IEEE Spectrum,* 1990, 38-39.
4. Verspecht J., *IEEE Trans. Instrum. Meas.*, 1995, **44**, 991-997.
5. Henderson D., Roddie A. G., Smith A. J. A., *IEE Proceedings-A*, 1992, **139**, 254-260.
6. Larson D. R., Paulter N. G., *Proc. 17th IEEE Instrumentation and Measurement Technology Conference, IMTC 2000,* Baltimore, USA, 1-4 May 2000, 1425-1428.
7. Verspecht J., *IEEE Trans. Instrum. Meas.*, 1994, **43**, 210-215.
8. Pintelon R., Schoukens J., *IEEE Trans. Instrum. Meas.*, 1996, **45**, 588-593.

9. Stenbakken G. N., Deyst J. P., *IEEE Trans. Instrum. Meas.*, 1998, **47**, 1056-1061.
10. Wang C. M., Hale P. D., Coakley K. J., *IEEE Trans. Instrum. Meas.*, 1999, **48**, 1324-1332.
11. IEC 469-2: *International Electrotechnical Commission, Pulse Techniques and Apparatus, Part 2: Pulse Measurement and Analysis, General Considerations*, 1987.
12. Taylor B. N., Kuyatt C. E., *Guidelines for evaluating and expressing the uncertainty of NIST measurement results*, NIST Technical Note 1297, Washington, D.C., U.S. Dept. of Commerce, 1994.
13. Larson D. R., Paulter N. G., *Temperature effects on the high-speed response of digitizing sampling oscilloscopes*, NCSL International, 2000 Workshop and Symposium, Toronto, Canada, 16-20 July 2000.
14. Souders T. M., Waltrip B. C., Laug O. B., Deyst J. P., *IEEE Trans. Instrum. Meas.*, 1997, **46**, 947-953.
15. Dabózi T., Kollár I., *IEEE Trans. Instrum. Meas.*, 1996, **45**, 417-421.
16. Roy S., Souders T. M., *Proc. 17th IEEE Instrumentation and Measurement Technology Conference, IMTC 2000*, Baltimore, USA, 1-4 May 2000, 1429-1434.
17. Gans W. L., *IEEE Trans. Instrum. Meas.*, 1983, **IM-32**, 126-133.
18. Mittermayer C., Steininger A., *IEEE Trans. Instrum. Meas.*, 1999, **48**, 1103-1107.
19. Paulter N. G., Larson D. R., *Time-base setting dependence of pulse parameters using high-bandwidth digital sampling oscilloscopes*, NCSL International, 2000 Workshop and Symposium, Toronto, Canada, 16-20 July 2000.

Received on 27 September 2001 and in revised form on 3 January 2002.

Glossary of terms

Synonymous meanings: measured, acquired, or sampled waveform

Not-reported variables

c_i	partial differential equation
g	transient amplitude gain-correction term
L_1	low reference level (for example, the 10 % reference level)
L_{1-}	data value found at $t_{L_{1-}}$
L_{1+}	data value found at $t_{L_{1+}}$
L_2	high reference level (for example, the 90 % reference level)
L_{2-}	data value found at $t_{L_{2-}}$
L_{2+}	data value found at $t_{L_{2+}}$
M_1	number of waveforms in DUT measurement set
M_2	number of reference pulse waveforms measured with sampler and used in sampler gain calibration
M_3	number of reference pulse waveforms measured with reference instrument and used in sampler gain calibration
M_4	number of temperature measurements taken during DUT measurement process
M_5	number of temperature measurements performed during sampler impulse response characterization
M_6	number of amplitude-temperature data pairs used to determine temperature effects on sampler's amplitude response or pulse generator's output amplitude
M_7	number of independent waveforms used to estimate transition duration of sampler step response, from control chart
M_8	number of transition duration-temperature data pairs used to determine temperature effects on sampler's transition duration response or pulse generator's output transition duration
M_9	number of $t_{d,m}V_{O,m}$ versus $t_{d,R}V_{O,R}$ data pairs used to calculate β_O curve
M_{10}	number of gain terms, from control chart
M_{11}	number of $t_{d,m}V_{U,m}$ versus $t_{d,R}V_{U,R}$ data pairs used to calculate β_U curve
M_{12}	number of jitter measurements, from control chart
M_{13}	number of amplitude versus time data pairs used to calculate duration of sampling interval
$m_{L_{1-}}$	time index for data having value closest to but $\leq L_1$
$m_{L_{1+}}$	time index for data having value closest to but $\geq L_1$
$m_{L_{2-}}$	time index for data having value closest to but $\leq L_2$
$m_{L_{2+}}$	time index for data having value closest to but $\geq L_2$
N_{bins}	number of bins in histogram
N_{S1}	bin number in histogram corresponding to lower state level mode bin
N_{S2}	bin number in histogram corresponding to upper state level mode bin
P_1	percentage of pulse amplitude for reference level L_1
P_2	percentage of pulse amplitude for reference level L_2
$S_{\delta t/\Delta T}$	temperature-dependent change in pulse transition duration
$S_{\Delta V/\Delta T}$	temperature-dependent change in pulse amplitude
T	temperature
T_{meas}	temperature at which a particular waveform was recorded
T_{ref}	average temperature over which a set of waveforms was recorded
$t_{d,m}$	transition duration, acquired waveform
$t_{d,r}$	transition duration, sampler step response estimate convolved with jitter
$t_{d,R}$	transition duration, reconstructed waveform
t_{L_1}	L_1 reference-level instant
$t_{L_{1-}}$	data instant preceding t_{L_1}
$t_{L_{1+}}$	data instant following t_{L_1}
t_{L_2}	L_2 reference-level instant

$t_{L,2_-}$	data instant preceding $t_{L,2}$
$t_{L,2_+}$	data instant following $t_{L,2}$
$V_{A,c}$	pulse amplitude, corrected waveform
$V_{A,m}$	pulse amplitude, acquired waveform
$V_{A,m,r}$	pulse amplitude, acquired waveform, reference pulse
$V_{A,R}$	pulse amplitude, reconstructed waveform
$V_{A,r}$	pulse amplitude, reference-instrument acquired waveform, reference pulse
$V_{S1,c}$	lower state level, corrected waveform
$V_{S1,m}$	lower state level, acquired waveform
$V_{S1,m,r}$	lower state level, acquired waveform, using reference pulse and sampler
$V_{S1,R}$	lower state level, reconstructed waveform
$V_{S1,r,r}$	lower state level, acquired waveform, using reference pulse and reference measurement instrument
$V_{max,m}$	maximum value, acquired waveform
$V_{max,R}$	maximum value, reconstructed waveform
$V_{min,m}$	minimum value, acquired waveform
$V_{min,R}$	minimum value, reconstructed waveform
$V_{S2,c}$	upper state level, corrected waveform
$V_{S2,m}$	upper state level, acquired waveform
$V_{S2,m,r}$	upper state level, acquired waveform, using reference pulse and sampler
$V_{S2,R}$	upper state level, reconstructed waveform
$V_{S2,r,r}$	upper state level, acquired waveform, using reference pulse and reference measurement instrument
$V_{O,m}$	overshoot value, acquired waveform
$V_{O,R}$	overshoot value, reconstructed waveform
$V_{U,m}$	undershoot value, acquired waveform
$V_{U,R}$	undershoot value, reconstructed waveform
$V_{\Delta T}$	temperature-induced incremental change in pulse amplitude
X_d	non-integer number of sampling intervals in transition duration of reconstructed waveform
X_j	non-integer number of sampling intervals in transition duration of effective jitter step response
X_m	non-integer number of sampling intervals in transition duration of acquired waveform
X_r	non-integer number of sampling intervals in transition duration of sampler step response waveform
β_O	overshoot correction factor relating transition duration of measured and reconstructed waveforms
β_U	undershoot correction factor relating transition duration of measured and reconstructed waveforms
$\Delta t_{d,\Delta T}$	temperature-induced incremental change in transition duration
ΔV	histogram bin size
δt	sampling interval
ν_{eff}	effective degrees of freedom
ν_i	degrees of freedom

Reported variables

O	overshoot value
U	undershoot (preshoot) value
t_d	transition duration
V_A	pulse amplitude, reported
u_i	uncertainty of the i-th variable

Institute of Physics Publishing Metrologia
Metrologia 43 (2006) 121–128 doi:10.1088/0026-1394/43/1/017

Some effects of temperature variation on sampling oscilloscopes and pulse generators

Donald R Larson[1] and Nicholas G Paulter Jr[1]

Quantum Electrical Metrology Division, NIST, Gaithersburg, MD 20899-8172, USA

Received 15 September 2005
Published 22 December 2005
Online at stacks.iop.org/Met/43/121

Abstract
The effects of temperature variation on the timebase errors and impulse responses of two 50 GHz bandwidth sampling oscilloscopes and on the pulse parameters of two pulse generators commonly used for oscilloscope calibrations are reported. The observed variations are significant for high accuracy measurements and contribute to the uncertainty of any measurements performed.

1. Introduction

Equivalent time, sampling oscilloscopes are now commercially available with 3 dB attenuation bandwidths exceeding 50 GHz. Pulse generators with transition durations of less than 16 ps are also commercially available. These high speed sampling oscilloscopes and pulse generators are used to make measurements needed to characterize high speed communications networks and components. These measurements are often made in locations where the temperature may change by several degrees Celsius between measurements. We have observed that the sampling heads and pulse generators may show differences due to changes in the ambient temperature. Furthermore, the uncertainties in the measurements may mean the difference between meeting specifications and failing an expensive network component.

2. Measurement set-up

We tested two different manufacturers' oscilloscope mainframes together with four different sampling heads and two different step generators. One sampling oscilloscope mainframe is identified as SM1 and the two sampling heads used with it are identified as SH1 and SH2. SH1 is a 50 GHz (3 dB attenuation bandwidth) sampling head and SH2 is a 20 GHz bandwidth sampling head. Similarly, the other sampling oscilloscope mainframe is identified as SM2 and the sampling heads used with it are identified as SH3 and SH4. SH3 and SH4 are, respectively, a 50 GHz (3 dB attenuation bandwidth) sampling head and a 20 GHz bandwidth sampling head. Each of these oscilloscopes was tested with two different manufacturers' step generators having a nominal bandwidth of 20 GHz. The step generators are identified as SG1 and SG2.

Before making any measurements, all instruments were allowed to warm up for at least two hours after applying power. This warm-up period was determined by attaching a temperature sensor to the cases of several instruments and observing the temperature of the instruments as a function of time. The measurements were performed by placing the instrument under test (oscilloscope mainframe, step generator or sampling head) inside an environmental chamber. This environmental chamber is located inside a shielded room where the temperature is controlled to within 1 °C over the measurement period. Only the temperature of the instrument under test was intentionally varied. The other components were kept at room temperature, 23.0 °C ± 1 °C. The sampling heads were connected to the oscilloscope mainframes using cabled extender modules purchased from the manufacturers. The step generator was connected to the sampling head using a high bandwidth (approximately 26 GHz) coaxial cable approximately 0.5 m long. When the step generators were being evaluated, a 50 GHz bandwidth sampling head was used. The trigger signal source was also kept at room temperature. The trigger signal input was located in the mainframe of one oscilloscope model and in the sampling heads of the other model. The temperature sensor was

[1] Quantum Electrical Metrology Division, Electronics and Electrical Engineering Laboratory, National Institute of Standards and Technology, Technology Administration, Department of Commerce. Official contribution of the National Institute of Standards and Technology, not subject to copyright in the USA.

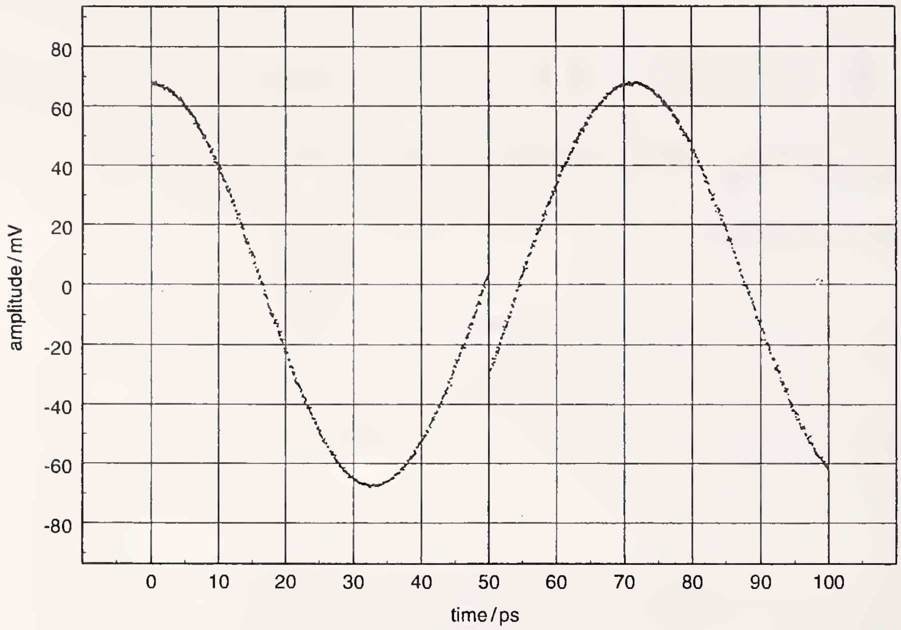

Figure 1. Waveform distortion caused by timebase error, 15 GHz sine wave.

a J type thermocouple and attached to the case of the instrument under test. The temperatures used in this work represent the manufacturers' narrowest specified operating temperature range (15 °C to 35 °C). The temperature was incremented in 5 °C steps. The instrument under test was kept at the target temperature for at least 30 min before measurements were made. In all cases, the temperature of the instrument varied by less than 0.2 °C during the measurements. At each set temperature, multiple waveforms were acquired, the parameters of interest determined and the mean and standard deviations of the parameters were calculated.

3. Sampling oscilloscope timebase errors

The timebase of a sampling oscilloscope generates an impressive range of epochs that can be varied from picoseconds to seconds, nine to eleven orders of magnitude. For the oscilloscope mainframes examined, the timebase consists of a startable oscillator and a time interpolator vernier (fine delay ramp) that has a delay range equal to one period of the startable oscillator. The timebase can be viewed as a repeated concatenation of the time interpolator vernier at every cycle of the startable oscillator until the desired epoch is achieved [1]. Unless the range of the time interpolator vernier is exactly one period of the startable oscillator, the sampling instant immediately after the concatenation occurs may differ from the intended sampling instant by several picoseconds. This timing error may produce a visible error in the waveform (figure 1). The time interpolator vernier, which has a range of several nanoseconds, is not perfectly linear and timing errors are also seen in that range. The non-linearity of the time interpolator vernier will also distort the waveform but this distortion is usually not obvious when observing an acquired waveform. The timing errors due to the non-linearity of the time interpolator vernier can be separated into two components, a fixed error in the reported sampling interval and a variable timing error that varies throughout the range of the time interpolator vernier. This first error component leads to the overall slope seen in the timebase error (figure 2). Although the second error component varies over the range of the time interpolator vernier, it varies the same way in each concatenation and can be seen as the repeating pattern in figure 2.

NIST has developed a method to characterize these timing errors [2] which has been used to obtain the results presented here. To summarize this technique, the single-frequency output from a synthesized sine-wave source is connected to the sampling oscilloscope and two or more unique waveforms are acquired. Each acquired waveform has a different phase relative to the trigger. The acquired waveforms are then compared to a theoretical sine wave and the residuals, divided by the derivative of the theoretical sine wave, yield the timebase error. The timebase error is the deviation of the actual time from the sampler reported time (intended time) as a function of the sampler reported time. It is evident from figures 1 and 2 that these timebase errors may impact measured pulse parameters [3].

To characterize the temperature dependence of the timebase error, an oscilloscope mainframe was placed in the environmental chamber while the 50 GHz bandwidth sampling head remained outside the environmental chamber at room temperature. The oscilloscope mainframe was allowed to come to thermal equilibrium by waiting 45 min before acquiring timebase data. A set of sine waves were acquired (two frequencies and multiple phases) and then the temperature was set to the next target temperature. This procedure was followed for both the mainframes tested. A subset of the results obtained is depicted in figures 3 and 4. The measurement

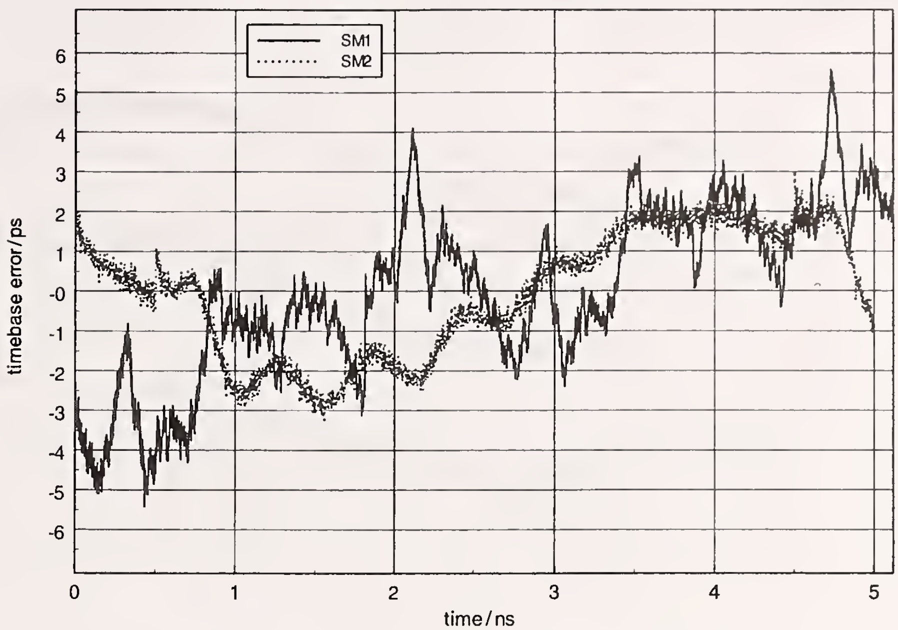

Figure 2. Timebase errors for SM1 and SM2 sampling oscilloscopes.

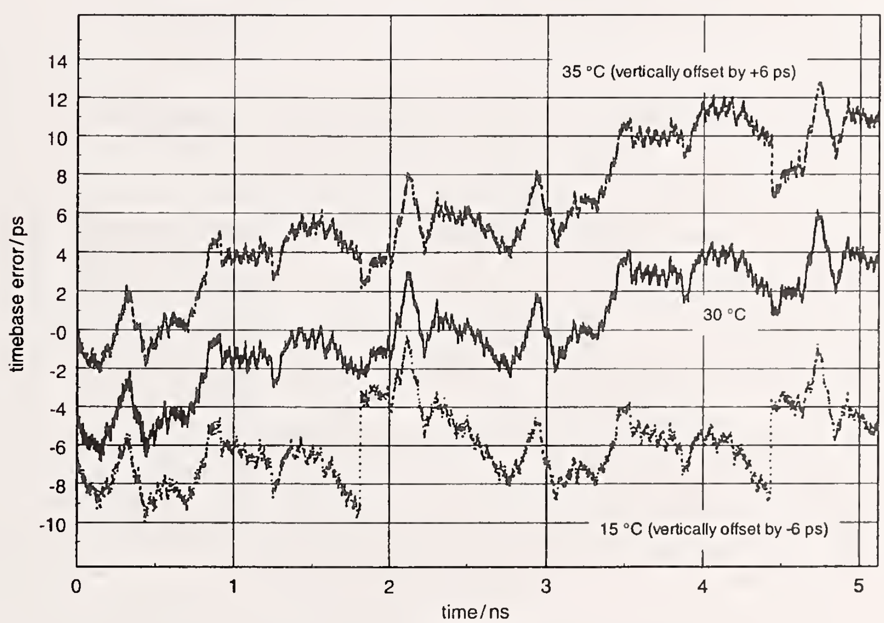

Figure 3. Timebase error for SM1 oscilloscope at three temperatures.

uncertainty corresponding to a 95% confidence interval is ± 0.08 ps. The concatenation error for SM1 (see figure 3) is seen to go through a minimum and change sign near 30 °C. Over the range of temperatures used, the timebase error for SM2 (see figure 4) did not go through a similar minimum but decreased monotonically. The error in the reported sampling interval changes for both mainframes as indicated by the tilt of the graph of the error estimate. The variation of the non-linearity appears to be nearly constant with temperature for both mainframes.

4. Pulse parameters

The pulse amplitude, high state, low state and transition durations (10% to 90% and 20% to 80%) were determined according to the procedures outlined in IEEE Standard 181-2003 [4]. A histogram of the data is first created and the two maxima of the resulting bimodal distribution define the high state and the low state. The number of histogram bins used for the data presented here was 4096. The amplitude is the difference between the high state and the low state.

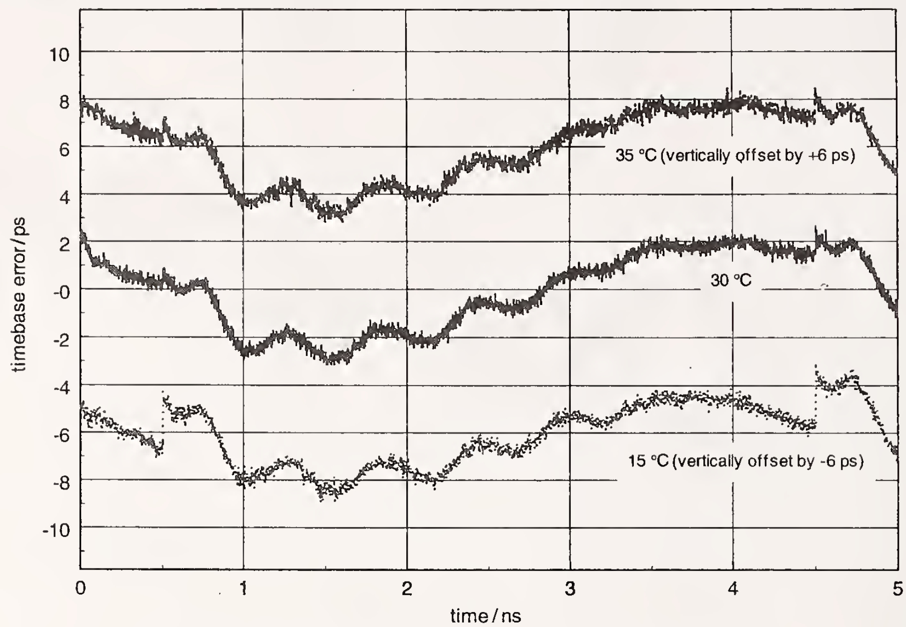

Figure 4. Timebase error for SM2 oscilloscope at three temperatures.

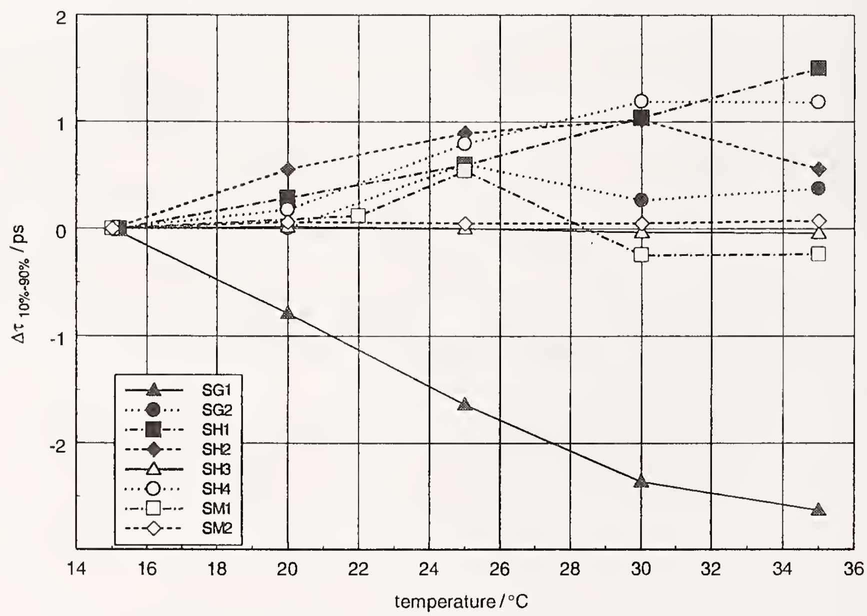

Figure 5. Change in transition duration (10% to 90%) as a function of temperature.

The 10%, 20%, 80% and 90% reference levels are calculated and their occurrence instants found by linear interpolation. The transition duration is the difference between the occurrence instants of the appropriate percentage reference levels.

The change in transition duration (10% to 90%) of all eight devices as a function of temperature is depicted in figure 5. Sampling heads SH1, SH2 and SH4 exhibited a small increase in transition duration (decrease in bandwidth) with increasing temperature. The transition duration of the waveform from step generator SG1 decreased significantly with temperature. Step generator SG2 exhibited only a small increase in transition duration with increasing temperatures. As previously mentioned, a set of data was obtained at each temperature; the maximum standard deviation observed in these sets of data was 0.206 ps.

Although the 10% to 90% transition duration is the most quoted pulse parameter, the 20% to 80% transition duration is included here and in the calibrations we perform. The 20% to 80% transition duration is affected less by aberrations than the 10% to 90% transition duration and, consequently,

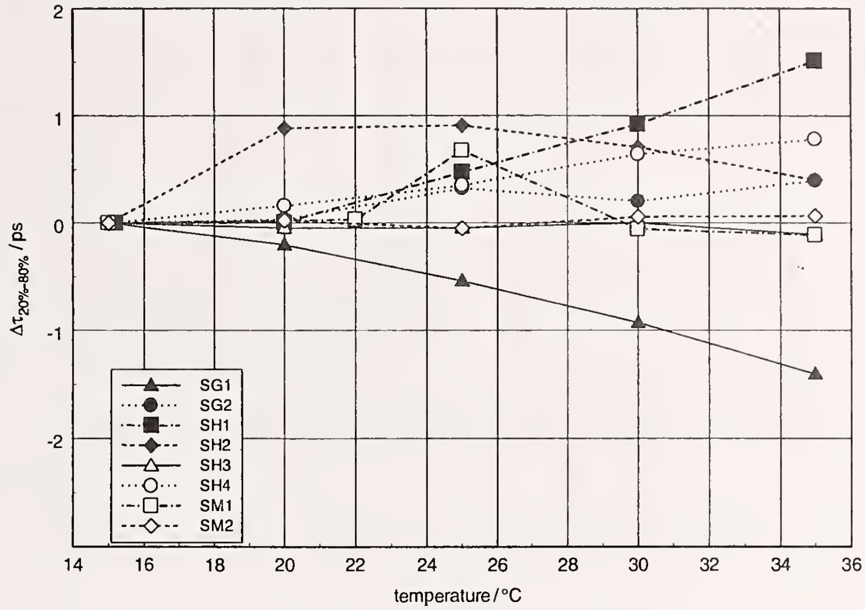

Figure 6. Change in transition duration (20% to 80%) as a function of temperature.

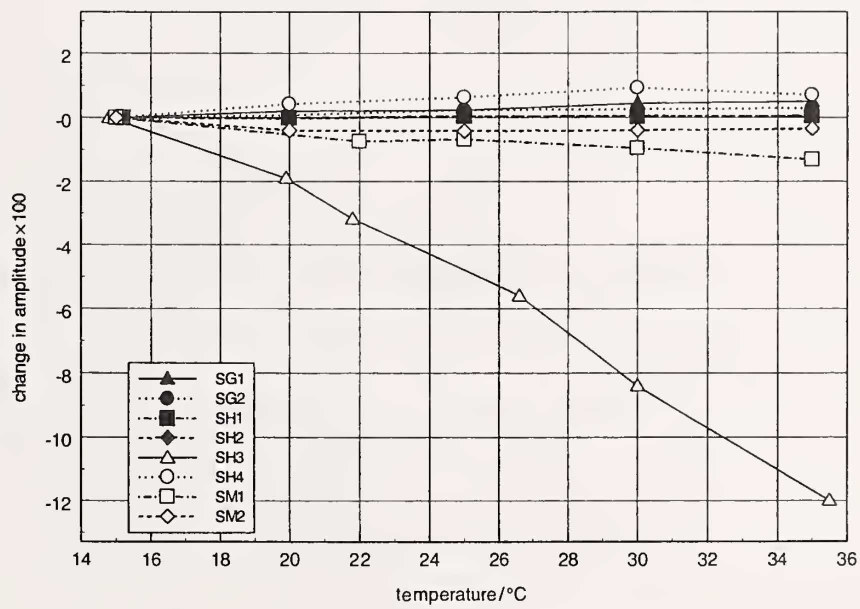

Figure 7. Change in amplitude (percentage) as a function of temperature.

often exhibits a smaller standard deviation. Figure 6 depicts the temperature dependence of the transition duration (20% to 80%) for all devices tested. These results were similar to the results for the 10% to 90% transition duration. The maximum standard deviation observed in any of the (20% to 80%) transition duration data sets is 0.130 ps.

Another parameter used to describe a pulse is the pulse amplitude. When the temperature is varied, both sampler gain and offset can vary. Figure 7 displays the amplitude changes we measured. SH3 displayed an unusually large decrease in amplitude with increasing temperature. To confirm this behaviour, a second sampling head of the same make and model was also tested with similar results. The other sampling heads and step generators exhibited increasing step amplitudes with increasing temperature. SH1 and SH2 (from the same manufacturer) were almost temperature invariant. For all the amplitude data reported here, the maximum standard deviation of a data set was 0.455 mV for a nominal pulse amplitude of 245 mV.

The changes in the voltage level associated with the high state and the voltage level associated with the low state were also examined and are depicted in figures 8 and 9. For sampling

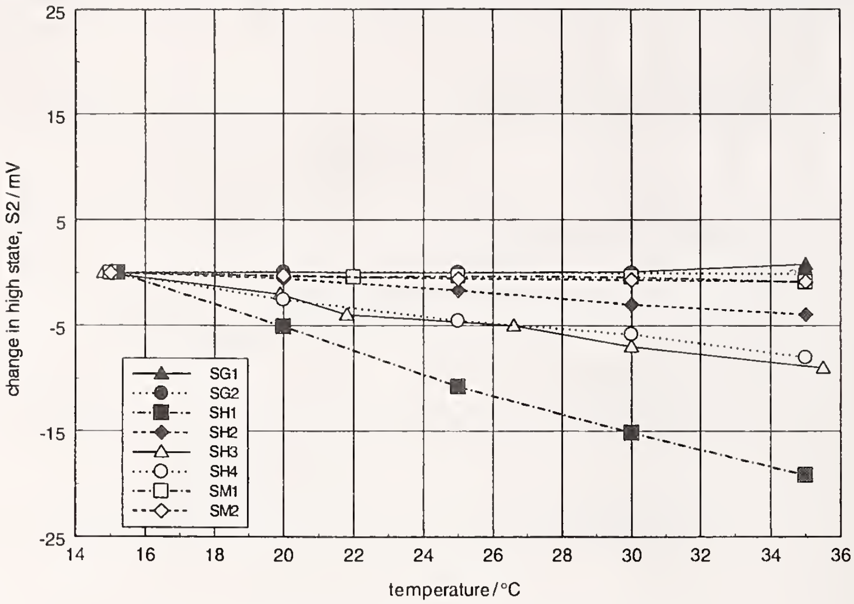

Figure 8. Changes in the high state, S2, as a function of temperature.

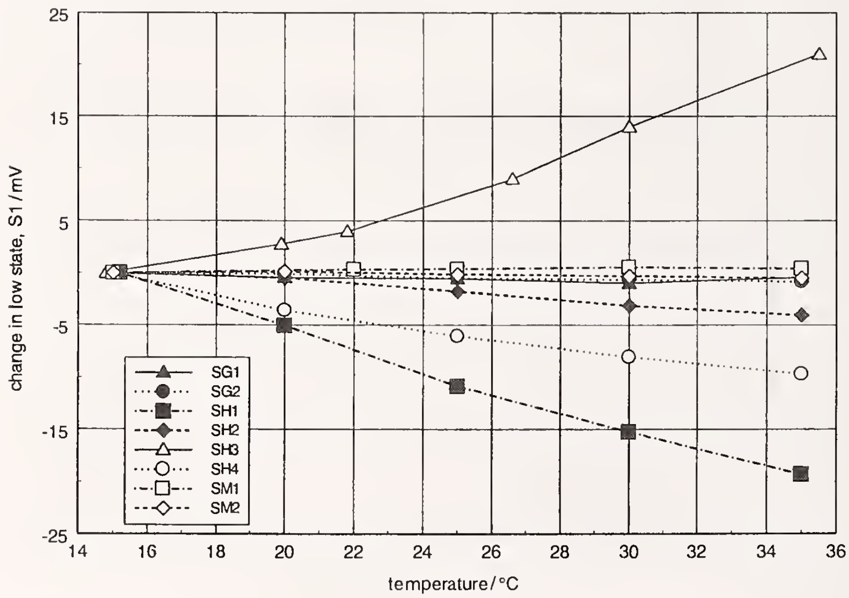

Figure 9. Changes in the low state, S1, as a function of temperature.

heads SH1, SH2 and SH4, the low states shifted to lower values as the temperature increased. However, because the high states exhibited a shift nearly equal to the low state shift and in the same direction, the change in amplitude (figure 7) for waveforms measured with these sampling heads is small. SH3, on the other hand, exhibited both a relatively large change in amplitude and offset. A waveform measured with this sampling head exhibited a decrease in amplitude and offset magnitude as the temperature increased.

The change in pulse parameters as a function of temperature for each device tested is summarized in table 1. Each entry is the slope of a straight line fit to the data for that particular step generator, sampling head or oscilloscope mainframe.

5. Transition occurrence instant

The position of the pulse in the epoch was also observed to change with temperature when the sampling oscilloscope mainframe, sampling head or pulse generator temperature varied. Figure 10 depicts the change in the transition occurrence instant (50% reference level instant) as a function

Table 1. Change in pulse parameters as a function of temperature, linear fit to data.

	High state slope/ (mV/°C)	Low state slope/ (mV/°C)	Amplitude slope/ (mV/°C)	10% to 90% transition duration slope/(ps/°C)	20% to 80% transition duration slope/(ps/°C)
SG1	0.033	−0.026	0.059	−0.137	−0.071
SG2	−0.006	−0.043	0.037	0.020	0.019
SH1	−0.976	−0.983	0.007	0.076	0.080
SH2	−0.206	−0.214	0.008	0.032	0.016
SH3	−0.435	1.043	−1.478	−0.003	−0.003
SH4	−0.385	−0.477	0.093	0.068	0.041
SM1	−0.037	0.024	−0.061	−0.017	−0.007
SM2	−0.040	−0.027	−0.014	0.003	0.003

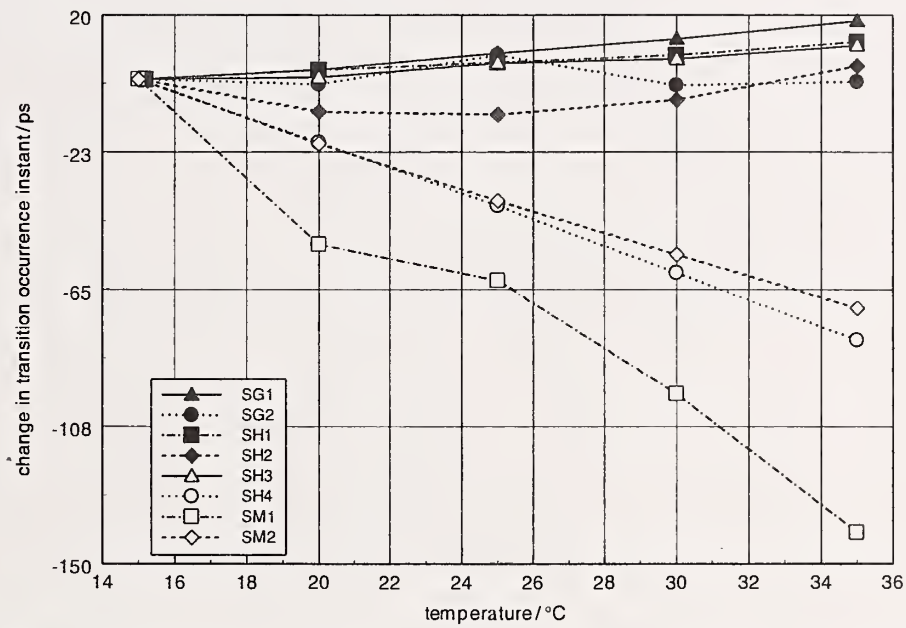

Figure 10. Change in transition occurrence instant (50% reference level instant) as a function of temperature.

of temperature. The maximum observed standard deviation for all instruments was 0.44 ps. For the sampling heads and pulse generators, this is independent of the temperature dependence of the timebase error or trigger signal since the oscilloscope mainframe temperature was held constant for those measurements. However, the large change in transition occurrence instant observed for SH4 is probably due to the trigger signal being routed through the sampling head. The changes observed for SM1 and SM2 are much too large to be the result of the change in the timebase error. Under certain conditions, the observed change in transition occurrence instant will have a significant effect on the transition duration. For example, if the temperature changes while a pulse waveform is being acquired and further, if the embedded waveform averaging routine is being used, the transition duration will increase as a result of this temperature-induced change in transition occurrence instant. It should be noted that the transition duration results presented previously were obtained at set temperatures and the small standard deviation of the measurements indicates that the change in transition occurrence instant was not a significant factor. This is indicative of a well-controlled environment, a necessity for a metrology facility involved in calibrating pulse generators and samplers.

6. Jitter

When making pulse waveform measurements, the acquired waveforms are impacted by the presence of trigger or system jitter. As with drift of the transition occurrence instant, averaging waveforms acquired in the presence of jitter will increase the transition duration. The effect on transition duration may be removed by measuring the jitter, modelling it with a Gaussian distribution and deconvolving the Gaussian distribution model from the acquired waveforms before determining the pulse parameters [5]. Because the measurements reported here are comparative, we did not remove jitter from any of the waveforms used. Consequently, the transition duration values will exhibit effects of the temperature dependence of jitter. However, the observed changes in jitter were much less than the uncertainty in our transition duration values. For SM1, the average jitter was less than 1.5 ps with a maximum standard deviation of 0.06 ps and varied less than 0.2 ps over the range of temperatures examined. For SM2, the average jitter was less than 1.0 ps with a maximum standard deviation of 0.02 ps and varied less than 0.03 ps over the temperature range used.

7. Summary

Changes in the error of the oscilloscope timebase have been characterized for two manufacturers' sampling oscilloscopes, both commonly used to characterize high speed digital communications networks and components. The changes in pulse parameters with temperature have been determined for two step generators, four sampling heads and two sampling oscilloscope mainframes. The transition duration measured by each sampling head increased (a bandwidth decrease) as the temperature increased except SH3 which displayed almost no change. Step generator SG1 produced a pulse with a faster transition duration (bandwidth increase) with increasing temperature. The step amplitudes for SG1, SG2, SH1, SH2, SH4, SM1 and SM2 were nearly insensitive to temperature changes, although level shifts were observed. This indicates a change in offset with temperature. No statistically significant changes in trigger or system jitter were observed. Changes in the pulse aberrations of overshoot and undershoot were also observed but are not reported here. Temperature-induced changes in pulse parameters and transition occurrence instant can contribute significantly to the uncertainty estimate [6, 7]. The results indicate a need for a well-controlled environment, typical of good metrology facilities, for pulse parameter measurements with low uncertainties. Although the results from the two sampling heads of the same model were similar, they were sufficiently different that each instrument had to be individually characterized. We note that when comparing measurement results from different laboratories using identical equipment or from the same laboratory but at different temperatures, the relative temperature differences must be known in order to explain the differences in results. Both sampling oscilloscopes examined here incorporated an embedded sampling head calibration routine. These routines were executed only once, before any measurements were made.

Acknowledgments

We wish to thank T M Souders for his technical comments. This work was partially funded by the US Air Force Calibration Coordination Group.

References

[1] Dobos L 1994 Advancements in picosecond resolution time interval measurement techniques *Conf. on Precision Electromagnetic Measurements (Boulder, CO, 27 June–1 July 1994)* pp 13–14

[2] Stenbakken G N and Deyst J P 1998 Time-base nonlinearity determination using iterated sine-fit analysis *IEEE Trans. Instrum. Meas.* **47** 1056–61

[3] Paulter N G Jr and Larson D R 2000 Time-base setting dependence of pulse parameters using high-bandwidth digital sampling oscilloscopes *National Conf. of Standards Laboratories International (Toronto, ON, Canada, 16–20 July)*

[4] IEEE Std 181-2003 *IEEE Standard on Transitions, Pulses and Related Waveforms* (New York: IEEE) pp 19, 24

[5] Gans W L 1983 The measurement and deconvolution of time jitter in equivalent-time waveform samplers *IEEE Trans. Instrum. Meas.* **IM-32** 126–33

[6] Larson D R and Paulter N G Jr 2000 Temperature effects on the high speed response of digitizing sampling oscilloscopes *National Conf. of Standards Laboratories International (Toronto, ON, Canada, 16–20 July)*

[7] Paulter N G and Larson D R 2002 Pulse parameter uncertainty analysis *Metrologia* **39** 143–55